TEXTURE ANALYSIS OF MAMMOGRAMS FOR CLASSIFICATION OF BREAST TISSUE DENSITY

Project report submitted in partial fulfillment of the requirement for the degree of

MASTER OF TECHNOLOGY

IN

ELECTRONICS & COMMUNICATION ENGINEERING

UNDER THE GUIDANCE OF

Dr. JITENDRA VIRMANI

BY

KRITI (132015)

May 2015

JAYPEE UNIVERSITY OF INFORMATION TECHNOLOGY
Waknaghat, Solan, Himachal Pradesh– 173234

Candidate's Declaration

I hereby declare that the work titled **"Texture Analysis of Mammograms for Classification of Breast Tissue Density"** carried under the guidance of Dr. Jitendra Virmani in partial fulfillment for the award of degree of Master of Technology in Electronics and Communication Engineering to Jaypee University of Information Technology, Waknaghat-Solan has not been submitted partially or wholly to any other University or Institute for the award of this or any other degree or diploma.

Date: Signature of Student

This is to certify that the above statement made by the candidate is correct to the best of my knowledge.

Date: Signature of Supervisor

Acknowledgement

This project work is the most significant accomplishment of my life by far. I would like to extend my gratitude and heartfelt thanks to my supervisor Dr. Jitendra Virmani, Assistant Professor (Sr. Grade), Department of Electronics and Communication Engineering, Jaypee University of Information Technology, Waknaghat-Solan, for his constant support, encouragement, exemplary guidance and constructive criticism.

Date: Name and Signature of Student

Table of Contents

List of Figures

List of Tables

List of Acronyms

ANN	Artificial Neural Network
ASM	Angular Second Moment
BI-RADS	Breast Imaging Reporting and Data System
CAD	Computer Aided Diagnosis
CM	Confusion Matrix
D	Dense
DDSM	Digital Database of Screening Mammograms
DG	Dense-Glandular
DWT	Discrete Wavelet Transform
FOS	First Order Statistics
F	Fatty
FG	Fatty-Glandular
FPS	Fourier Power Spectrum
GLDS	Gray Level Difference Statistics
GLCM	Gray Level Co-occurrence Matrix
GLRLM	Gray Level Run Length Matrix
GWT	Gabor Wavelet Transform
ICA	Individual Class Accuracy
kNN	*k*-Nearest Neighbor
KSFD	Kernel Self Fisher Discriminant
LDA	Linear Discriminant Analysis
MIAS	Mammographic Image Analysis Society
MLO	Medio-Lateral Oblique
NGTDM	Neighborhood Gray Tone Difference Matrix
NN	Neural Network
OCA	Overall Classification Accuracy
PC	Principal Component
PCA	Principal Component Analysis
PNN	Probabilistic Neural Network
ROIs	Regions of Interest
RTFV	Reduced Texture Feature Vector
SIFT	Scale-Invariant Feature Transform
SFM	Statistical Feature Matrix
SFS	Sequential Feature Selection
SSVM	Smooth Support Vector Machine
SVM	Support Vector Machine
TEM	Texture Energy Measures
TFV	Texture Feature Vector
WPT	Wavelet Packet Transform

Abstract

The most common form of cancer being diagnosed in women worldwide is breast cancer. It has been well established that the risk of breast cancer development is associated with increased breast density. Therefore, characterization of breast tissue density is clinically significant. The radiologists predict the breast tissue density by visual analysis which is highly subjective. Moreover, the differential diagnosis between atypical cases of breast tissue where there is significant overlap in appearance on mammographic images is a daunting challenge even for experienced radiologists. Therefore, there is a significant impetus among the research community to develop computer aided diagnostic (CAD) systems for differential diagnosis between different cases of breast tissue density patterns.

Thus, in order to provide the radiologists with a second opinion tool for validating their diagnosis, various CAD systems have been developed in the present work for two-class and three-class breast tissue density classification.

A general framework of the different CAD schemes employed in the present work is shown in Figure 1. For the design of this CAD system, 322 mammographic images are taken from the MIAS dataset. From each mammographic image, ROIs of fixed size are extracted. The CAD system consists of feature extraction module, feature space dimensionality reduction module and the classification module. In the feature extraction module, three methods for extracting the texture features are employed, (*a*) Statistical methods (*b*) Signal processing based method and (*c*) Transform domain based methods. Each feature set is normalized by using min-max normalization. The normalized feature set is then bifurcated into training and testing datasets.

In the feature space dimensionality reduction module, redundant and correlated texture features are eliminated by applying Principal component analysis (PCA). In the first step PCA is carried out on the training dataset and reduced training dataset of the derived PCs is obtained. The reduced testing dataset is then obtained by projecting the data points of training dataset in the direction of the PCs of training dataset.

In the classification module, performance of four different classifiers namely kNN, probabilistic neural network (PNN), SVM and smooth support vector machine (SSVM) is evaluated to obtain the class of the unknown testing instances.

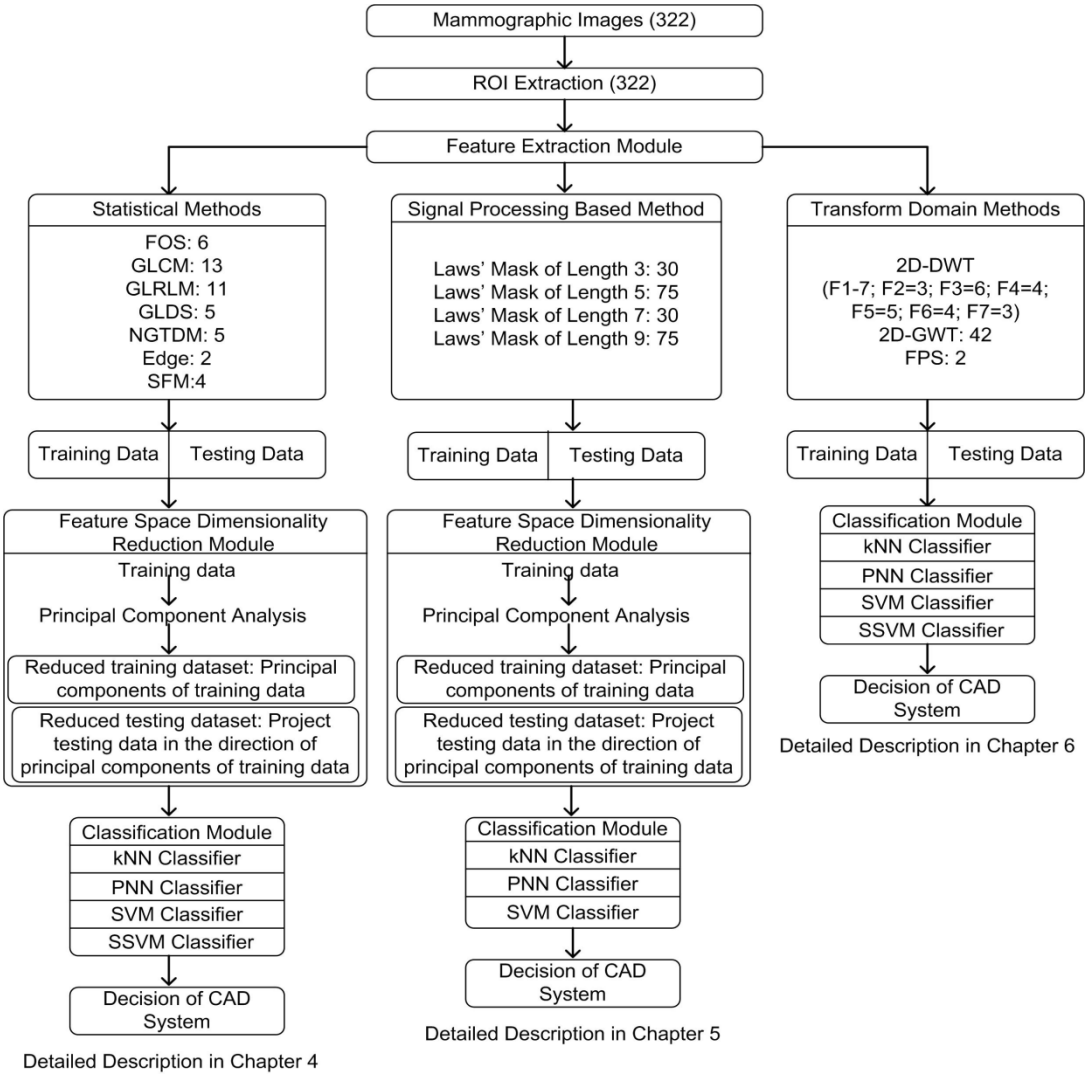

Figure 1 General framework of the proposed CAD system design.
Note: FOS: First order statistics, GLCM: Gray level co-occurrence matrix, GLRLM: Gray level run length matrix, GLDS: Gray level difference statistics, NGTDM: Neighbourhood gray tone difference matrix, SFM: Statistical feature matrix, DWT: Discrete wavelet transform, GWT: Gabor wavelet transform, FPS: Fourier power spectrum.

In *Chapter 4* a CAD system based on statistical features is developed for two-class and three-class breast tissue density classification of mammograms.

In *Chapter 5* a CAD system based on texture features derived from Laws' masks of various lengths has been designed for two-class and three-class breast tissue density classification of mammograms.

In *Chapter 6* performance of various multiresolution texture features is evaluated for two-class and three-class breast tissue density classification of mammograms.

Chapter 1

Introduction

1.1. Overview

Cancer comes under a class of diseases that are characterized by uncontrolled growth of cells resulting in formation of tissue masses called tumors at any location in the body [1]. The malignant tumor can destroy other healthy tissues in the body and often travels to other parts of the body to form new tumors. This process of invasion and destruction of healthy tissues is called metastasis [2]. Breast cancer is the type of cancer that develops form breast cells. It is considered to be a major health problem nowadays and is the most common form of cancer found in women [3]. For the women in United Kingdom, the lifetime risk of being diagnosed with breast cancer is 1 in 8 [4]. The study in [5] reported 1.67 million new incidences of breast cancer worldwide in the year 2012. There are various risk factors associated with cancer development: (*a*) Age, (*b*) History of breast cancer, (*c*) Formation of certain lumps in the breasts (*d*) Higher breast density, (*e*) Obesity, (*f*) Alcohol consumption, (*g*) Cosmetic implants.

It has been strongly advocated by many researchers in their study that increased breast density is strongly correlated to the risk of developing breast cancer [6-14]. The association between increased breast density and breast cancer risk can be explained on the basis of effects due to the hormones mitogens and mutagens. The size of the cell population in the breast and cell proliferation is affected by mitogens while the likelihood of damage to these cells is due to mutagens. Due to increased cell population, there is an increase in reactive oxygen species (ROS) production and lipid peroxidation. The products of lipid peroxidation; malondialdehyde (MDA) and isoprostanes catalyze the proliferation of cells [14]. The schematic overview of the above process is depicted in Figure 1.1.

Even though breast cancer is considered to be a fatal disease with a high mortality rate, the chances of survival are significantly improved if detected at an early stage. There are various imaging modalities like ultrasound, MRI, Computerized tomography, etc. that can be used for diagnosing the breast diseases but mammography is considered to be the best choice for detection due to its higher sensitivity [15-17].

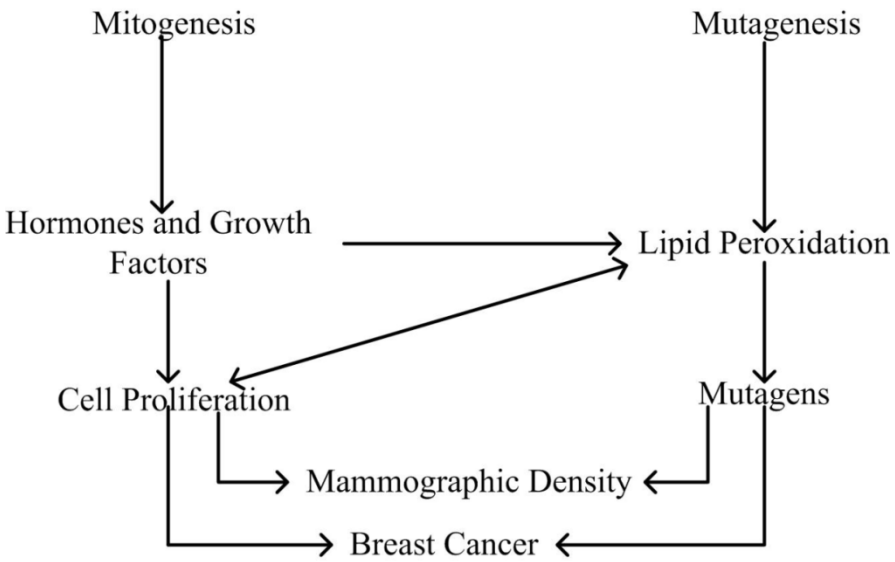

Figure 1.1 Schematic overview of processes resulting in increased breast density and thus increased risk of developing breast cancer.

1.2. Mammography

Mammography is an x-ray imaging technique used to detect any abnormalities in the breast. There are two types of mammography examination:

(*a*) Screening Mammography: Screening mammography is used to check for breast abnormalities in asymptomatic women. This examination is used to detect breast cancer at an early stage when there are no symptoms present.

(*b*) Diagnostic Mammography: Diagnostic mammography is performed when either a patient has complaint of some lumps in the breast, pain or any abnormality is detected during the screening process. It helps in determining whether the symptoms indicate the presence of a malignancy and is also used to find the exact location of the abnormalities.

Mammograms display the adipose (fatty) and fibroglandular tissues of the breast along with the present abnormalities. To describe the findings on the mammograms, The American College of Radiology came up with a standard system called Breast Imaging Reporting and Data System (BI-RADS). The categories were [18]:

(*i*) *Category 0*: Additional imaging evaluation- If any abnormality is present, it may not be clearly noticeable and more tests are needed.

(*ii*) *Category 1*: Negative- No abnormalities found to report.

(*iii*) *Category 2*: Benign finding- The finding in the mammogram is non-cancerous like lymph nodes.

(*iv*) *Category 3*: Probably benign finding- The finding is most probably non-cancerous but is expected to change over time so a follow up is required regularly.

(*v*) *Category 4*: Suspicious abnormality- The findings might or might not be cancerous so to find the exact nature of the finding, the patient should consider taking a biopsy test.

(*vi*) *Category 5*: Highly suggestive malignancy- The finding has more than 95 % chance of being cancerous and biopsy examination is highly recommended for the patient.

(*vii*) *Category 6*: Known biopsy-proven malignancy- The findings on the mammogram have been shown to be cancerous by a previous biopsy.

On the basis of density, breast tissue can be classified into the following categories:

(*a*) *Fatty (F) / Dense (D) (Two-class classification)*

(*b*) *Fatty (F) / Fatty-glandular (FG) / Dense-glandular (DG) (Three-class classification)*

(*c*) *Almost entirely fatty (B-I) / Some fibro-glandular tissue (B-II) / Heterogeneously dense breast (B-III) / Extremely dense breast (B-IV) (Four-class BI-RADS classification)*

The typical fatty tissue being translucent to X-rays appears dark on a mammogram where as the dense tissues appear bright on the mammograms. The fatty-glandular breast tissue is an intermediate stage between fatty and dense tissues therefore a typical fatty-glandular breast tissue appears dark with some bright streaks on the mammogram. The mammographic appearances of the breast tissue based on density are depicted in Figure 1.2.

For BI-RADS reporting, B-I: breast contains very little fibroglandular tissue. B-II: Some of the areas of the breast contain fibroglandular tissue. B-III: Breast contains very little adipose tissue and there are more regions of fibroglandular tissue. B-IV: Almost complete breast consists of fibroglandular tissue. The typical mammographic appearances of the breast tissue based on BI-RADS reporting are shown in Figure 1.3.

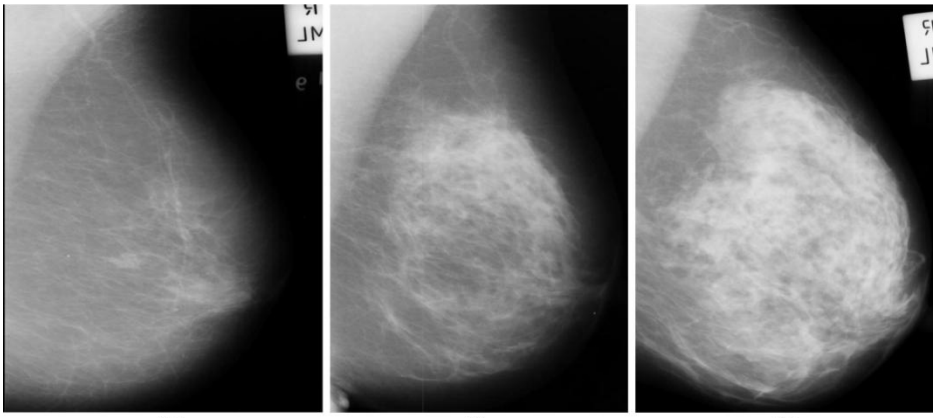

Figure 1.2 Appearances of breast tissue density patterns on mammograms (*a*) Fatty tissue, (*b*) Fatty-glandular tissue, (*c*) Dense-glandular tissue.

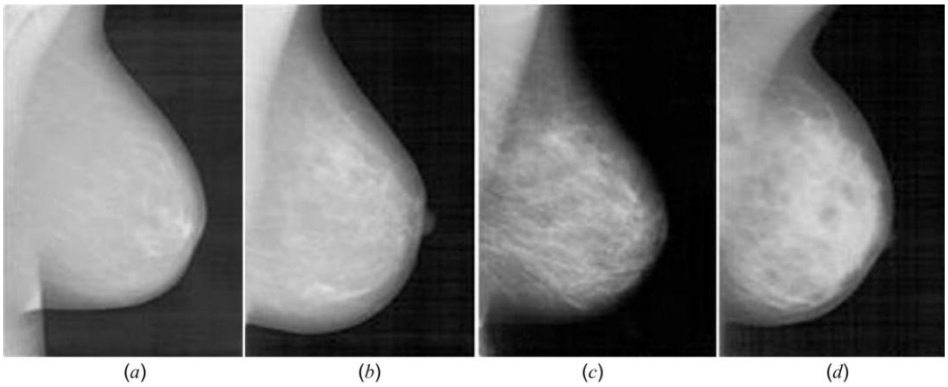

Figure 1.3 Appearances of breast tissue density patterns based on BI-RADS reporting (*a*) B-I tissue, (*b*) B-II tissue, (*c*) B-III tissue, (*d*) B-IV tissue.

1.3. Need of Computer Aided Diagnostic Systems

With the advancement in computer technology and artificial intelligence techniques there has been a substantial increase in the opportunities for researchers to investigate the potential of computer-aided diagnostic (CAD) systems for texture analysis and tissue characterization of radiological images [19-22]. Tissue characterization refers to quantitative analysis of the tissue imaging features resulting in accurate distinction between different types of tissues. Thus, the result of tissue characterization is interpreted using numerical values. The overall aim of developing a computerized tissue characterization system is to provide additional diagnostic information about the underlying tissue which cannot be captured by visual inspection of medical images.

The mammograms are visually analyzed by the radiologists to identify and differentiate between different density patterns of the breast tissue. The typical breast tissue density patterns are easy to identify and analyze. This analysis is however subjective and depends on the experience of the radiologist. The appearances of atypical cases of the breast tissue density patterns are highly overlapping and to differentiate between these atypical cases through visual analysis is considered to be a highly daunting task for the radiologists. Thus, in order to provide the radiologists with a second opinion tool for validating their diagnosis, various CAD systems have been developed for breast tissue density classification. The sample images depicting the typical and atypical cases of breast tissue density patterns are shown in Figure 1.4 and Figure 1.5, respectively.

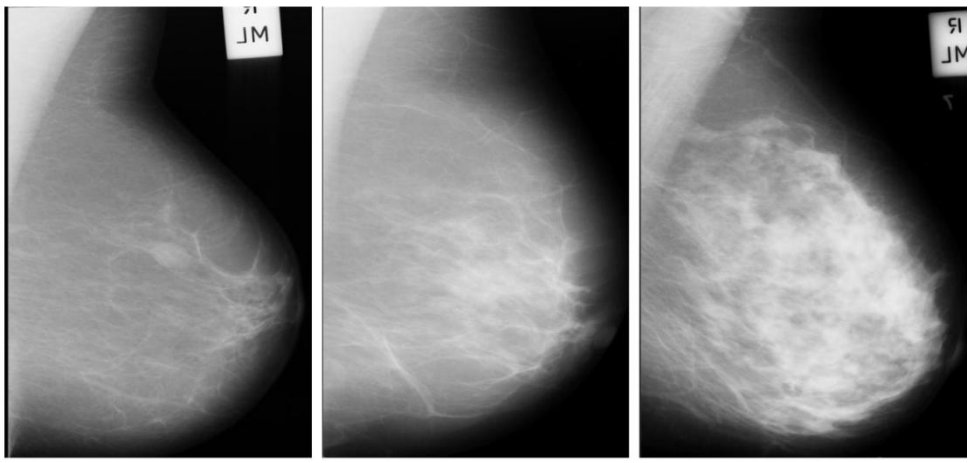

Figure 1.4 Sample mammographic images depicting typical cases. (*a*) Typical fatty tissue 'mdb012' (*b*) Typical fatty-glandular tissue 'mdb014' (*c*) Typical dense-glandular tissue 'mdb108'.

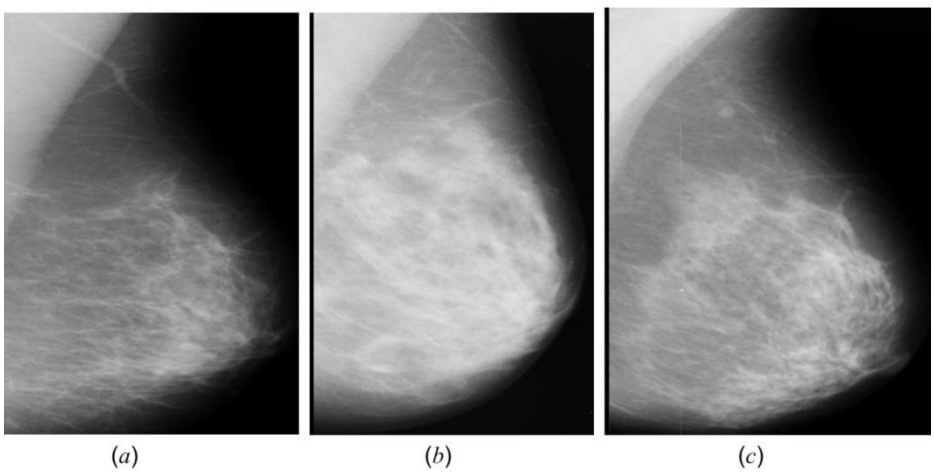

Figure 1.5 Sample mammographic images depicting atypical cases (*a*) Atypical fatty tissue 'mdb088', (*b*) Atypical fatty-glandular tissue 'mdb030' (*c*) Atypical dense-glandular tissue 'mdb100'.

1.4. Objective of the Present Study

The main objective of the research work presented in this project report is to enhance the diagnostic potential of mammographic images for identification of different breast tissue density patterns by developing efficient CAD system designs using a representative image database. The various research objectives formulated for the present work are described below:

(*i*) *The collection of a comprehensive and representative database*: To develop efficient CAD systems, it is necessary that the classifiers used in the classification module of the CAD system are trained with an image database that contains representative images from each subclass. Thus collection of a comprehensive database containing representative images for different breast tissue density patterns like (*a*) fatty breast tissue, (*b*) fatty-glandular breast tissue and (*c*) dense-glandular breast tissue is considered as the first objective of the present research work.

(*ii*) *The design and development of an efficient CAD system for two and three class breast tissue density classification*: The risk of developing breast cancer is strongly correlated with the increased breast tissue density, therefore for early detection of breast cancer risk; it is clinically significant to determine the density of the breast tissue first. Due to overlapping appearances of the breast tissue density patterns, the subjective analysis of the mammograms is a confusing and difficult task for the radiologists and it is believed that a CAD system that predicts the density pattern of the breast tissue acts as a second opinion tool for the radiologists in validating their diagnosis. Therefore, design of a CAD system for classification between different breast tissue density patterns is taken up as the next objective of the present research work.

1.5. Organization of Report

(*i*) *Chapter 1* lays the foundation as to why analysis and classification of breast tissue density patterns is clinically significant. The chapter begins with the documenting facts about breast cancer, recent statistics related to breast cancer among women worldwide, risk factors that can lead to the development of breast cancer, correlation between breast cancer risk and increased breast tissue density, mammographic appearances of different breast density patterns, different classification categories into which breast tissue density patterns are divided. The chapter also focuses on the need

of CAD systems and how they contribute towards the analysis of mammograms. What are the main objectives of the present work and how are they formulated.

(*ii*) *Chapter 2* presents a brief review of the other related studies carried out for classification of breast tissue density patterns using mammographic images.

(*iii*) *Chapter 3* focuses on the research methodology that is followed for undertaking the present research work. This chapter gives a description of the image database used in the CAD system, the protocol followed to extract ROIs form each image. Various modules of the proposed CAD system are also explained in detail.

(*iv*) *Chapter 4* gives a detailed description of the proposed CAD system design for breast tissue density classification using statistical features.

(*v*) *Chapter 5* describes in detail the proposed CAD system for breast tissue density classification using Laws' texture features.

(*vi*) *Chapter 6* describes the CAD system for breast tissue density classification using features derived from transform domain based methods of texture feature extraction.

(*vii*) *Chapter 7* summarizes the conclusion drawn from the experimentation carried out in the present research work on "Texture Analysis of Mammograms for Classification of Breast Tissue Density". The chapter also reports the future scope for the extension of this work.

Chapter 2

Literature Review

2.1. Introduction

Characterization of breast tissue according to different density patterns is clinically significant because the high breast tissue density is associated with the risk of developing breast cancer. The radiologists after analyzing the mammograms predict the breast tissue density but this visual analysis is highly subjective. For atypical cases, the differential diagnosis between breast issue density patterns is difficult as there is a significant overlap in the appearances on the mammographic images and it is considered to be daunting challenge even for experienced radiologists. Therefore there is a huge impetus among various researchers to develop CAD systems useful for differentiating between breast tissue density patterns.

The research works reported in related studies have proposed various CAD system designs for breast tissue density classification. These proposed CAD systems can be categorized as: (*a*) CAD system designs based on segmented breast tissue v/s CAD system designs based on Regions of Interest (ROIs). (*b*) CAD system designs for two class classification (fatty/dense) v/s CAD system designs for three class classification (fatty/fatty-glandular/dense-glandular) v/s CAD system designs for four class classification based on BI-RADS (B-I: almost entirely fatty/B-II: some fibro-glandular tissue/B-III: heterogeneously dense breast/B-IV: extremely dense breast). (*c*) CAD system designs using standard benchmark dataset (Mammographic image analysis society (MIAS), Digital database of screening mammograms (DDSM), Oxford, Nijmegen) v/s CAD system designs using data collected by individual research groups. A brief description of the related studies is given as follows.

2.2. Different CAD System Designs for Two-Class Breast Tissue Density Classification

Various researchers in the past have developed different CAD systems for classifying the breast tissue density patterns into two classes namely fatty and dense. A brief description of these related studies is given in Table 2.1.

Table 2.1: Summary of studies carried out for two-class breast tissue density classification

Investigators	Dataset Description				
	Database	**No. of Images**	**ROI Size**	**Classifier**	**OCA (%)**
Miller et al. [23]	Collected by investigator	40	SBT	Bayesian	80.0
Bovis et al. [24]	DDSM (SBMD)	377	SBT	ANN	96.7
Castella et al. [25]	Collected by investigator	352	256 × 256	LDA	90.0
Oliver et al. [26]	MIAS (SBMD)	322	SBT	Bayesian	91.0
	DDSM (SBMD)	831			84.0
Mustra et al. [27]	MIAS (SBMD)	322	512 × 384	Naïve Bayesian	91.6
	KBD-FER (Collected by investigator)	144		IB1	97.2
Sharma et al. [28]	MIAS (SBMD)	322	200 × 200	SMO-SVM	96.4
Sharma et al. [29]	MIAS (SBMD)	212	200 × 200	kNN	97.2

Note: SBMD: Standard benchmark database. SBT: Segmented breast tissue OCA: Overall Classification Accuracy.

Miller et al. [23] proposed a classification algorithm to classify a set of 40 mammograms into fatty or dense categories using Laws' mask features of length 5 to characterize the texture. The features were extracted after pre-processing of the images to remove the background and pectoral muscle. The extracted features were then fed to a Bayesian classifier to categorize the test images achieving the highest classification accuracy of 80.0 %.

Bovis et al. [24] proposed an approach based on fusion of classifiers to classify the mammographic images as fatty or dense. The study was carried out on 377 mammograms taken from the DDSM database. The images were pre-processed for segmenting the breast tissue from the background and segmented breast tissue was used for feature extraction. The extracted features were contrast, homogeneity, correlation, sum average, sum variance, entropy, sum entropy, difference average, difference variance, information measure of correlation-1, information measure of correlation-2, inertia, variance and angular second moment derived from Spatial gray level dependency (SGLD) matrices; total spectral energy using Fourier power spectrum (FPS); total texture energy from Laws' texture masks; standard deviation, mean, skewness and kurtosis using Discrete wavelet transform (DWT); statistical features like entropy, standard deviation, mean, skewness and kurtosis; a circularity shape feature; fractal dimensions i.e. Hurst coefficient. Principal component analysis (PCA) was then used for feature space dimensionality reduction and first 30 Eigen values i.e. principal components (PCs) were found to be sufficient to classify the

mammograms. These PCs were then fed to a set of artificial neural network (ANN) classifiers and an accuracy of 96.7 % was obtained.

Castella et al. [25] proposed a scheme to classify 352 digital mammograms taken from Clinique des Grangettes, Geneva as per BI-RADS categories. The B-I and B-II BI-RADS categories were combined to form fatty class while the BI-RADS categories B-III and B-IV were combined to form dense class. From the mammographic images ROIs of size 256 × 256 pixels were selected. The extracted features were balance, standard deviation, skewness and kurtosis derived from gray level histogram; energy, entropy, cmax, contrast, homogeneity derived using gray level co-occurrence matrix (GLCM); short primitive emphasis, long primitive emphasis, primitive length uniformity, gray level uniformity derived from primitive matrix; a fractal dimension using fractal analysis; coarseness, contrast, complexity, strength derived using neighborhood gray tone difference matrix (NGTDM). This feature vector was used for classification of mammograms using Bayesian, Naïve Bayesian and Linear discriminant analysis (LDA) classifiers. The highest classification accuracy of 90.0 % was achieved using LDA classifier for two class classification problem.

Oliver et al. [26] proposed a CAD system to classify mammograms taken from the MIAS database and the DDSM database into fatty or dense categories reduced by combining the BI-RADS categories. The mammograms were pre-processed to remove pectoral muscle, background and labels. The breast region was segmented into two clusters using fuzzy C-means clustering and morphological and texture features were extracted from each cluster. Morphological features include relative area, first four histogram moments (mean, standard deviation, skewness, kurtosis). Texture features like contrast, energy, correlation, entropy, sum average, difference average, sum entropy, difference entropy and homogeneity were extracted using GLCM. This feature set was then fed to the decision tree, Bayesian and *k*- nearest neighbor (kNN) classifiers. The study reported the highest overall classification accuracy of 91.0 % using Bayesian classifier.

Mustra et al. [27] proposed a scheme to classify the mammograms taken from two different databases: (*a*) The MIAS database and (*b*) KBD-FER database into fatty or dense categories. The images were pre-processed and segmented and then ROI of size 512 × 384 pixels was selected from each image. From the ROIs statistical features like contrast, correlation, autocorrelation, cluster shade, cluster prominence,

entropy, dissimilarity, energy, homogeneity, variance, sum variance, difference variance, sum average, sum entropy, difference entropy, information measure of correlation-1and information measure of correlation-2 were obtained from GLCM and features like number of pixels with higher intensity than muscle region, mean intensity, number of pixels with higher intensity than Otsu's threshold, standard deviation, entropy, kurtosis and skewness were extracted directly from the ROIs. Different wrapper based feature selection techniques were then used and the selected features were fed to nearest neighbor and naïve bayesian classifiers. The study reported highest classification accuracy of 91.6 % and 97.2 % using best first, backward selection method with naïve bayesian classifier for the MIAS database and IB1 classifier for the KBD-FER database, respectively.

Sharma et al. [28] proposed a classification algorithm to classify mammograms from the MIAS database into fatty or dense class. From these images, the ROIs of size 200 × 200 pixels were extracted from the center of the breast tissue behind the nipple as it is considered to be the densest region of the breast tissue. From these ROIs features were extracted using various texture models like angular second moment, difference variance, correlation, contrast, sum of squares, entropy, inverse difference moment, sum average, sum variance, sum entropy, difference entropy, information measure of correlation-1, information measure of correlation-2, maximal correlation coefficient from co-occurrence matrix; homogeneity, entropy, contrast, mean and energy from SGLDM; mean, variance, skewness, kurtosis from first order statistics (FOS); coarseness, contrast, periodicity, roughness from statistical feature matrix (SFM); edge-level, spot-level, wave-level, ripple-level, spot-edge, wave-edge, ripple-edge, wave-spot, ripple-spot, ripple-wave, edge-edge, spot-spot, wave-wave, ripple-ripple from Law' texture energy measures; Hurst coefficient at resolution 1, Hurst coefficient at resolution 2 from fractal analysis; radial sum and angular sum from Fourier power spectrum. Out of all the extracted features some features like correlation, inverse difference moment, entropy, mean, skewness, ripple-edge, Hurst coefficient and angular sum were selected using sequential feature selection (SFS) algorithm. The study reported an accuracy of 94.4 % using SMO-SVM classifier.

In yet another recent study Sharma et al. [29] presented an automated approach to classify 212 mammograms out of 322 mammograms of the MIAS dataset into fatty or dense classes has been proposed. From each mammogram, an ROI of size

200 × 200 pixels was extracted from the center of the breast. For texture analysis, Haralick's GLCM, SFM, GLDS, FOS, Law's texture energy measures (TEM), Fractal and FPS features were used. Out of these features, redundant features were removed using feature selection technique done by scalar feature ranking. The study reported an accuracy of 97.2 % with kNN classifier.

2.3. Different CAD System Designs for Three-Class Breast Tissue Density Classification

Different CAD system designs have been proposed in the recent past for classifying the mammograms into one of the three classes namely fatty, fatty-glandular and dense-glandular. A brief description of the related studies is given in Table 2.2.

Table 2.2: Summary of studies carried out for three-class breast tissue density classification

Investigators	Dataset Description				
	Database	No. of Images	ROI Size	Classifier	OCA (%)
Blot et al. [30]	MIAS (SBMD)	265	SBT	kNN	63.0
Bosch et al. [31]	MIAS (SBMD)	322	SBT	SVM	91.3
Muhimmah et al. [32]	MIAS(SBMD)	321	SBT	DAG-SVM	77.5
Subashini et al. [33]	MIAS (SBMD)	43	SBT	SVM	95.4
Tzikopoulos et al. [34]	MIAS (SBMD)	322	SBT	SVM	84.4
Li et al. [35]	MIAS (SBMD)	42	SBT	KSFD	94.4
Mustra et al. [27]	MIAS (SBMD)	322	512 × 384	IB1	82.0
Silva et al. [36]	MIAS (SBMD)	320	300 × 300	SVM	77.1

Note: SBMD: Standard benchmark database. SBT: Segmented breast tissue OCA: Overall Classification Accuracy.

Blot et al. [30] proposed an approach to classify 265 mammograms taken from the MIAS database into fatty, fatty-glandular or dense-glandular classes. The images were pre-processed to segment the breast tissue by removing the background and pectoral muscle. The segmented breast tissue was then used for extracting the features based on grey-level histograms from some selected regions of the breast. From the histogram of each region standard deviation and skewness are calculated as texture features. The study reported an overall classification of 63.0 % with kNN classifier.

Bosch et al. [31] presented an approach to classify the mammographic images taken from the MIAS database into fatty, fatty-glandular or dense-glandular classes. The images were preprocessed to extract the breast tissue and remove pectoral muscle and the background. From the segmented breast tissue, texture features were extracted

using scale-invariant feature transform (SIFT) and classification was carried out using support vector machine (SVM) classifier achieving an accuracy of 91.3 %.

Muhimmah et al. [32] proposed a CAD system using multiresolution histogram based texture features to classify 321 mammograms taken from the MIAS database into fatty, fatty-glandular or dense-glandular classes, using directed acyclic graph-support vector machine (DAG-SVM) classifier yielding the classification accuracy of 77.5 %.

Subashini et al. [33] proposed an approach for automatic assessment of breast tissue. The algorithm was tested on a subset of 43 mammograms taken from the MIAS database. The mammograms were pre-processed to remove artifacts and pectoral muscle. The feature extraction was then applied to the segmented breast and statistical features like mean, standard deviation, skewness, kurtosis, uniformity, smoothness, average histogram, modified standard deviation and modified skew were extracted for texture representation. The SVM classifier was used for classifying the images into fatty, fatty-glandular or dense-glandular classes obtaining an accuracy of 95.4 %.

Tzikopoulos et al. [34] used a CAD system for automatic segmentation and classification of breast tissue into fatty, fatty-glandular or dense-glandular classes. The proposed algorithm was tested on the MIAS database. The images were pre-processed and segmented to remove the noise and pectoral muscle. ROIs were then extracted using thresholding technique. From these ROIs statistical and fractal features were extracted. The study reported classification accuracy of 84.4 % using the SVM classifier.

Li et al. [35] proposed an approach to classify 42 normal mammograms taken out of 322 mammograms of the MIAS database into fatty, fatty-glandular or dense-glandular classes. The mammograms were preprocessed to remove the background, artifacts and pectoral muscle. From the segmented breast tissue, seven statistical features namely mean, smoothness, standard deviation, skewness, average histogram, uniformity and kurtosis were extracted. The study reported classification accuracy of 94.4 % using the Kernel self-optimized fisher discriminant (KSFD) classifier.

Mustra et al. [27] proposed an approach to automatically classify the mammograms taken from the MIAS database into fatty, fatty-glandular or dense-glandular classes. The images were pre-processed and segmented to extract an ROI of size 512 × 384 pixels from each image. From the ROIs statistical features like

contrast, correlation, autocorrelation, cluster shade, cluster prominence, entropy, dissimilarity, energy, homogeneity, variance, sum variance, sum average, sum entropy, difference entropy, difference variance, information measure of correlation-1 and information measure of correlation-2 were obtained from GLCM and features like number of pixels with higher intensity than muscle region, mean intensity, number of pixels with higher intensity than Otsu's threshold, standard deviation, entropy, kurtosis and skewness were extracted directly from the ROIs. Wrapper based feature selection method was then applied to this feature set and the selected features were then used for the classification task using the nearest neighbor and Naïve Bayesian classifier achieving maximum accuracy of 82.0 %.

Silva et al. [36] proposed a method to classify the 320 mammograms taken from the MIAS database into fatty, fatty-glandular and dense-glandular classes. From each mammogram, an ROI of size 300 × 300 pixels was extracted. From these ROIs statistical features like mean, standard deviation, smoothness, asymmetry, uniformity, kurtosis, average histogram, modified standard deviation and modified symmetry were extracted from the histograms and features like maximum probability, correlation, uniformity, homogeneity and entropy were extracted using the co-occurrence matrix. The study reported an accuracy of 77.1 % using the SVM classifier.

2.4. Different CAD System Designs for Four-Class Breast Tissue Density Classification

Various researchers in the past have proposed different CAD system designs in their study to classify the breast tissue into four classes as per BI-RADS reporting. A brief description of the related studies is given in Table 2.3.

Karssemeijer [37] proposed an automated approach for detection of breast density to classify the mammograms as per BI-RADS standard (B-I: almost entirely fatty breast, B-II: some fibroglandular tissue, B-III: heterogeneously dense breast, B-IV: extremely dense breast). To test the performance of the proposed approach 615 digital mammograms obtained from Nijmegen database were used. The images were pre-processed to remove background and pectoral muscle. Global thresholding technique was used for removal of background tissue and pectoral muscle was removed using straight line approximation. The feature set consists of 8 features including standard deviation and skewness calculated from histograms. The kNN

classifier has been used for the classification task and an accuracy of 65.0 % was reported.

Table 2.3: Summary of studies carried out for four-class breast tissue density classification

Investigators	Dataset Description				
	Database	No. of Images	ROI Size	Classifier	OCA (%)
Karssemeijer [37]	Nijmegen (SBMD)	615	SBT	kNN	80.0
Wang et al. [38]	Collected by investigator	195	SBT	NN	71.0
Petroudi et al. [39]	Oxford (SBMD)	132	SBT	Nearest neighbor	76.0
Oliver et al. [40]	DDSM (SBMD)	300	SBT	kNN+ID3	47.0
Bosch et al. [31]	MIAS (SBMD)	322	SBT	SVM	95.4
	DDSM (SBMD)	500			84.7
Castella et al. [25]	Collected by investigator	352	256 × 256	LDA	83.0
Oliver et al. [26]	MIAS (SBMD)	322	SBT	Bayesian	86.0
	DDSM (SBMD)	831			77.0
Mustra et al. [27]	MIAS (SBMD)	322	512 × 384	IB1	79.2
	KBD-FER (collected by investigator)	144			76.4

Note: SBMD: Standard benchmark database. SBT: Segmented breast tissue OCA: Overall Classification Accuracy.

Wang et al. [38] proposed a CAD system for automatically classifying the mammograms as per BI-RADS standard. The approach was tested on 195 mammograms acquired from the University of Pittsburgh Medical Centre. Thickness correction was applied to the mammograms. Features were extracted from the histograms obtained from the breast area. The extracted features included low intensity value of the image, ratio between low intensity value and high intensity value, ratio between initial and peak values to the total range of distance and ratio of number of pixels falling between the peak and the highest intensity values to the total number of pixels. These features were then fed to the neural network (NN) classifier to classify the breast tissue achieving highest accuracy of 71.0 %.

Petroudi et al. [39] proposed an approach for automatic classification of breast tissue density. The approach was tested on 137 mammograms collected from Oxford Database. Each mammogram was segmented into 3 components: breast tissue, background and pectoral muscle. After the removal of pectoral muscle and background, the segmented breast tissue was filtered using maximum response (MR8) filter bank. The filter responses were then clustered to form a texton dictionary. Using

this dictionary a texton histogram was formed for each mammogram in the training data. The histogram for testing data was compared to all known distributions and BI-RADS category for each mammogram was classified on the basis of nearest neighbor model using χ^2 distribution comparison achieving highest accuracy of 76.0 %

Oliver et al. [40] proposed a CAD system using a subset of 300 mammograms taken from the DDSM database for classification into BI-RADS categories. The mammograms were first segmented based on similarity in tissue appearance using fuzzy C-means clustering followed by feature extraction using morphological and texture features. As morphological features, center of masses, relative area, and mean intensity of clusters were calculated while texture features like contrast, energy, correlation, entropy, homogeneity, sum average, sum entropy, difference average and difference entropy were derived from GLCM. These features were then fed to kNN and decision tree classifiers achieving an accuracy of 47.0 % by combining both the classifiers.

Bosch et al. [31] proposed a CAD system design to classify the mammograms taken from the MIAS and DDSM databases as per BI-RADS categories. Each mammogram was preprocessed to extract the segmented breast tissue after removing the pectoral muscle and the background. From the segmented breast tissue, texture features were extracted using SIFT and classification was carried out using SVM and kNN classifiers. Highest accuracy of 95.4 % and 84.7 % was achieved for MIAS and DDSM database, respectively with SVM classifier.

Castella et al. [25] proposed a technique to classify 352 mammograms collected at Clinique des Grangettes into one of the four BI-RADS categories. From each mammogram four ROIs of size 256 × 256 pixels were selected and were used to extract the statistical features like balance, standard deviation, skewness and kurtosis derived from gray level histogram; energy, entropy, cmax, contrast, homogeneity derived using GLCM; short primitive emphasis, long primitive emphasis, primitive length uniformity , gray level uniformity derived from primitive matrix; a fractal dimension using fractal analysis; coarseness, contrast, complexity, strength derived using NGTDM. This feature vector was then fed to three classifiers namely Mahalanobis Bayesian, LDA and Naïve Bayesian and highest classification accuracy of 83.0 % was achieved using LDA classifier.

Oliver et al. [26] proposed a technique to classify the mammograms taken form MIAS and DDSM databases as per BI-RADS categories. The mammograms

were pre-processed to remove pectoral muscle, background and labels. The breast region was segmented into two clusters using fuzzy C-means clustering and morphological and texture features were extracted from each cluster. Morphological features include relative area, first four histogram moments (mean, standard deviation, skewness, kurtosis). Texture features like contrast, energy, entropy, correlation, sum average, sum entropy, difference average, difference entropy and homogeneity were extracted using co-occurrence matrices. The resultant feature vector was then fed to different classifiers like kNN, decision tree and bayesian. For the MIAS dataset, highest classification accuracy of 86.0 % was achieved with Bayesian classifier and for DDSM database, highest classification accuracy of 77.0 % was achieved with Bayesian classifier.

Mustra et al. [27] proposed an approach to automatically classify the mammograms taken from the MIAS database and KBD-FER database as per BI-RADS categories. The images were pre-processed and segmented to extract an ROI of size 512 × 384 pixels from each image. From the ROIs statistical features like contrast, correlation, autocorrelation, cluster shade, cluster prominence, entropy, dissimilarity, energy, homogeneity, variance, sum variance, sum average, sum entropy, difference entropy, difference variance, information measure of correlation-1 and information measure of correlation-2 were obtained from GLCM and features like number of pixels with higher intensity than muscle region, mean intensity, number of pixels with higher intensity than Otsu's threshold, standard deviation, entropy, kurtosis and skewness were extracted directly from the ROIs. Wrapper based feature selection method was then applied to this feature set and the selected features were then used for the classification task using the nearest neighbor and Naïve Bayesian classifier achieving maximum accuracy of 79.2 % for MIAS database using best first, backward selection technique and IB1 classifier. For the KBD-FER database, highest accuracy of 76.4 % was achieved with best first forward selection and IB1 classifier.

2.5. Concluding Remarks

From the above tables, it can be observed that most of the researchers have used a subset of MIAS and DDSM databases and have worked on the segmented breast tissue. It is also observed that only a few studies report CAD systems based on ROIs extracted from the breast [25, 27-29, 36] even though it has been shown [41] that the ROIs extracted from the centre of the breast result in highest performance as

this region of the breast is densest and extraction of ROIs also eliminates an extra step of preprocessing included in obtaining the segmented breast tissue for pectoral muscle removal.

Chapter 3

Methodology

3.1. Introduction

From the extensive literature survey presented in the previous chapter, it can be observed that most of the related studies carried out in the past are based on the pre-processing of mammograms to extract the segmented breast tissue after removing the pectoral muscle and the background while only a few studies report CAD systems based on ROIs extracted from the breast even though it has been shown [41] that the ROIs extracted from the center of the breast result in highest performance as this region of the breast is densest and extraction of ROI also eliminates an extra step of pre-processing included in obtaining the segmented breast tissue after removal of background and pectoral muscle removal. Thus in the present work, taking into consideration the effect of ROI size and location on performance of the algorithms, different CAD system designs are proposed for the classification of different breast tissue density patterns based on their underlying texture characteristics.

3.2. Proposed CAD System Designs for Classification of Breast Tissue Density Patterns

In the present work, various CAD system designs have been proposed to classify the different breast tissue density patterns. A general framework of the different CAD schemes employed in the present work is shown in Figure 3.1. For the design of this CAD system, a dataset of 322 mammographic images was taken. The CAD system consists of feature extraction module, feature space dimensionality reduction module and the classification module. In the feature extraction module, three methods for extracting the texture features are employed. (*a*) Statistical methods: In this statistical features based on FOS, 2^{nd} order statistics i.e. GLCM, Higher order statistics i.e. Gray level run length (GLRL) and other feature models like GLDS, NGTDM and SFM are computed. (*b*) Signal processing based method: In this method texture features are computed from each ROI using Laws' mask of different resolutions i.e. 3, 5, 7 and 9. (*c*) Transform domain methods: In this spectral features like 2D-DWT features, Gabor wavelet transform (GWT) features and FPS features are extracted from each ROI. Each feature set is normalized by using min-max

normalization. The normalized feature set is then bifurcated into training and testing datasets.

In the feature space dimensionality reduction module, redundant and correlated texture features are eliminated by applying PCA. In the first step PCA is carried out on the training dataset and reduced training dataset of the derived PCs is obtained. The reduced testing dataset is then obtained by projecting the data points of training dataset in the direction of the PCs of training dataset.

In the classification module, performance of four different classifiers namely kNN, probabilistic neural network (PNN), SVM and smooth support vector machine (SSVM) is evaluated to obtain the class of the unknown testing instances.

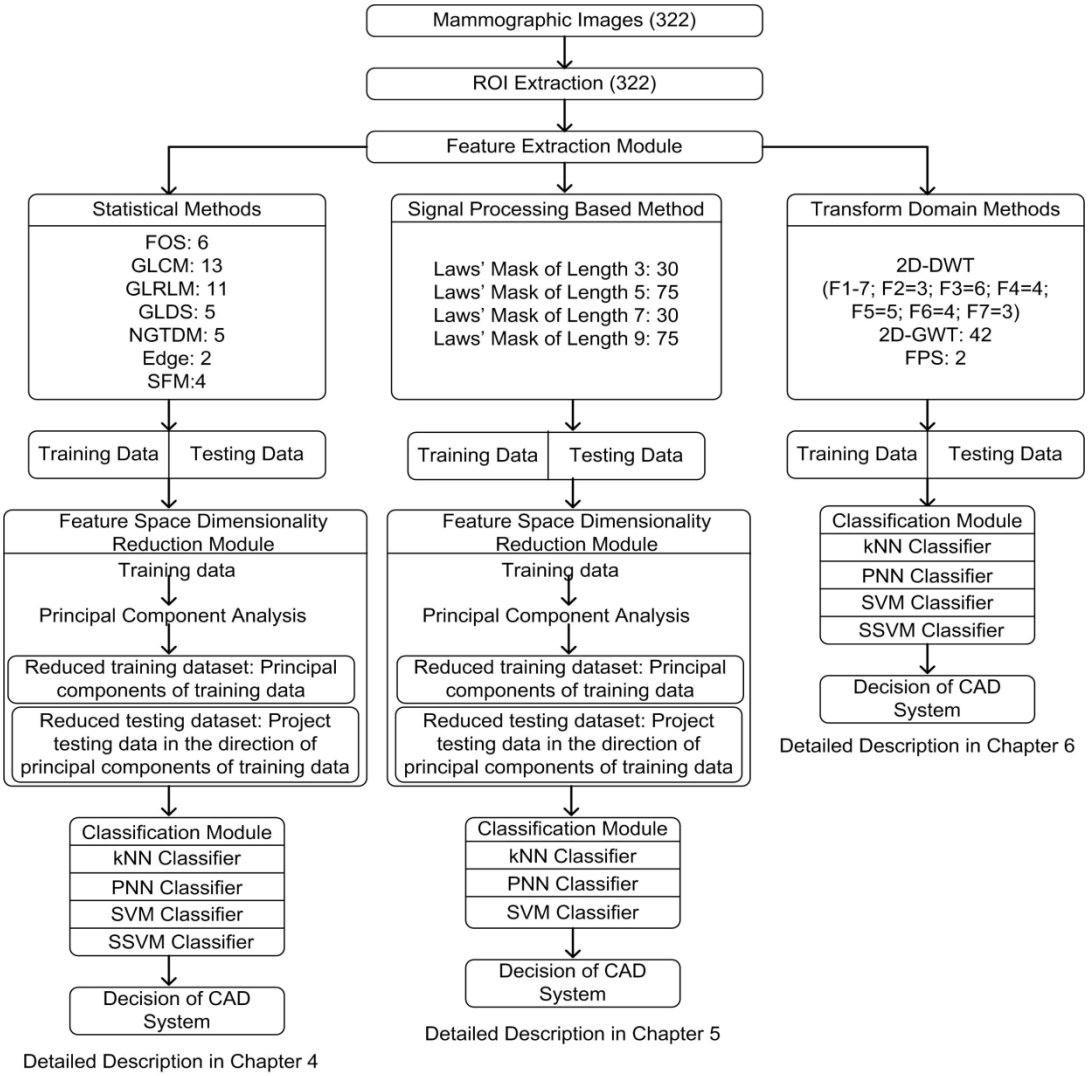

Figure 3.1 General framework of the proposed CAD system design.
Note: FOS: First order statistics, GLCM: Gray level co-occurrence matrix, GLRLM: Gray level run length matrix, GLDS: Gray level difference statistics, NGTDM: Neighbourhood gray tone difference matrix, SFM: Statistical feature matrix, DWT: Discrete wavelet transform, GWT: Gabor wavelet transform, FPS: Fourier power spectrum.

3.3. Dataset Description

In order to test the proposed CAD system design, a publicly available database: The mini-MIAS database has been used.

This database consists of the Medio Lateral Oblique (MLO) views of both the breasts of 161 women i.e. a total of 322 mammographic images. These images are selected from the UK National Breast Screening Programme and were digitized using The Joyce-Loebl scanning microdensitometer. The images in the database are categorized into three categories as per their density namely fatty (106 images), fatty-glandular (104 images) and dense-glandular (112 images). Each image in the database is of size 1024 × 1024 pixels, with 256 gray scale tones and a horizontal and vertical resolution of 96 dpi. The database also includes location of abnormality, the radius of the circle enclosing the abnormality, its severity and nature of the tissue [42]. In the present work CAD system designs have been proposed for (*a*) two-class breast tissue density classification i.e. (Fatty and Dense class) and (*b*) three-class breast tissue density classification i.e. (Fatty, fatty-glandular and dense-glandular classes). For implementing CAD systems for two-class breast tissue density classification, the fatty-glandular and dense-glandular classes are combined and considered as dense class resulting in 106 mammograms belonging to fatty class and 216 mammograms belonging to dense class. The description of the dataset, used for two-class and three-class CAD system designs is shown in Figure 3.2.

3.3.1. Selection of Regions of Interest (ROIs)

The ROI size is selected carefully considering the fact that it should provide a good population of pixels for computing texture features [42]. Different ROI sizes that have been selected in the literature for classification are 256 × 256 pixels [25], 512 × 384 pixels [27], 200 × 200 pixels [28, 29] and 300 × 300 pixels [36]. Other researchers have pre-processed the mammograms by removal of the pectoral muscle and the background using segmented breast tissue for feature extraction [23, 24, 26, 30-35, 37-40]. For the present work ROIs of size 200 × 200 pixels are manually extracted from each mammogram. The ROIs are selected from the center of the breast tissue as it has been asserted by many researchers in their research after having conducted various experiments that this area is the densest region of the breast and selecting ROI from this part of the breast results in highest performance of the

proposed algorithms [28, 29, 41]. The selection and extraction of ROI from the breast tissue is shown in Figure 3.3.

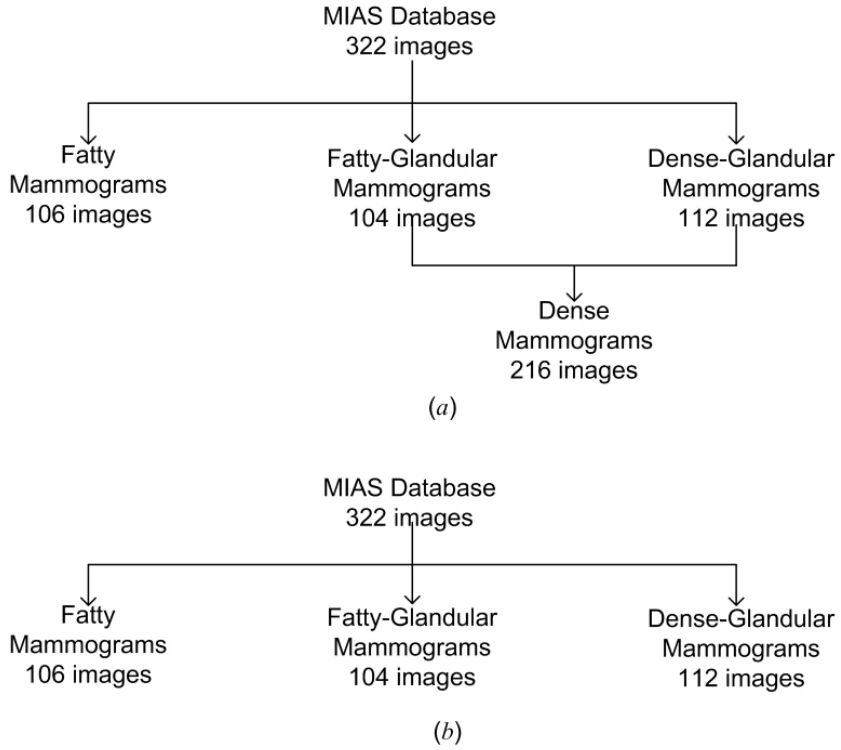

Figure 3.2 Dataset description (*a*) Two-class breast tissue density classification (*b*) Three-class breast tissue density classification.

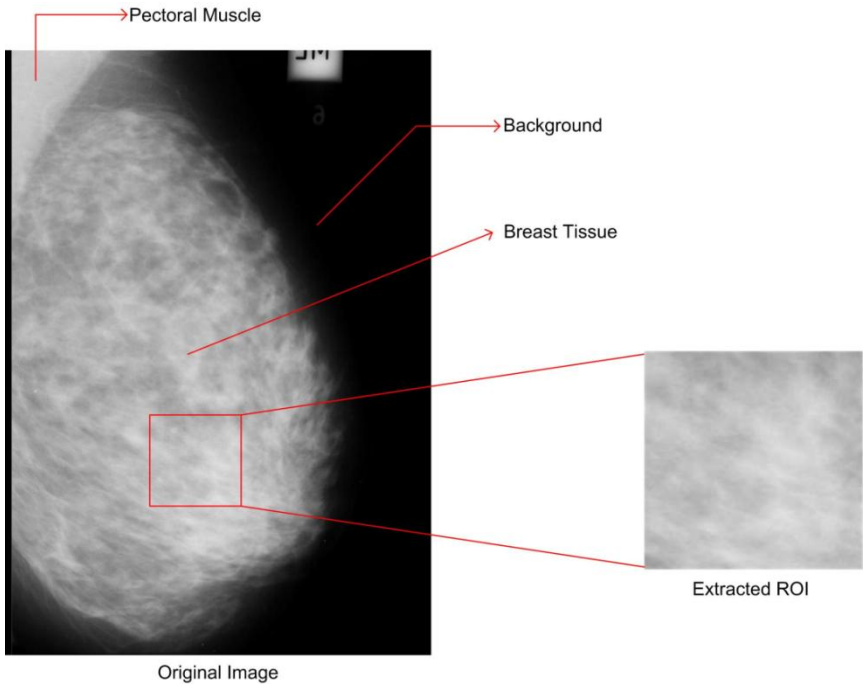

Figure 3.3 Sample mammographic image with ROI marked.

The sample images of ROIs extracted from the mammographic images are shown in Figure 3.4.

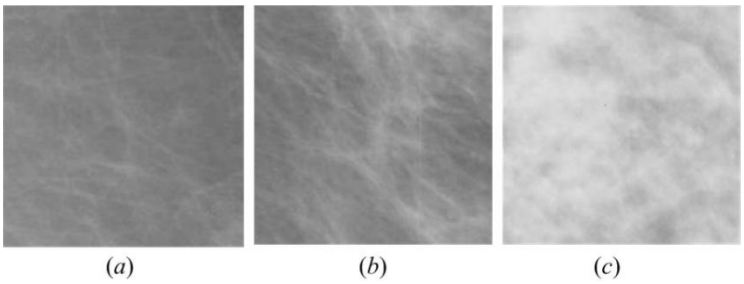

Figure 3.4 Sample ROI images. (*a*) Fatty tissue 'mdb012', (*b*) Fatty-glandular tissue 'mdb014', (*c*) Dense-glandular tissue 'mdb108'.

3.4. Feature Extraction Module

The feature extraction is the process used to transform the visually extractable and non-extractable features into mathematical descriptors. These descriptors are either shape-based (morphological features) or intensity distribution based (textural features). There are a variety of methods to extract the textural features including statistical, signal processing based and transform domain methods.

3.4.1. Statistical Methods

The statistical methods are used to extract the texture features from an image based on the gray level intensities of the pixels of that image. Based on the number of pixels used to compute the texture features, statistical methods can be classified into first-order statistics, second-order statistics and higher-order statistics.

3.4.1.1. First Order Statistics (FOS)

The first order statistics are derived from the gray level intensity histograms of the image. Six features namely average gray level, standard deviation, smoothness, kurtosis and entropy are computed for each ROI [43].

3.4.1.2. Second Order Statistics-GLCM Features

To derive the statistical texture features from GLCM, spatial relationship between two pixels is considered. The GLCM tabulates the number of times the different combinations of pixel pairs of a specific gray level occur in an image for various directions θ = 0°, 45°, 90°, 135° and different distances d=1, 2, 3 etc. Total 13 GLCM features namely angular second moment (ASM), contrast, correlation, inverse difference moment, variance, sum average, sum variance, difference variance, sum

entropy, entropy, difference entropy, information measures of correlation-1 and information measures of correlation-2 are computed from each ROI [44-46].

3.4.1.3. Higher Order Statistics-GLRLM Features

To derive the statistical texture features from the GLRLM, spatial relationship between more than two pixels is considered. In a given direction, GLRLM measures the number of times there are runs of consecutive pixels with the same value. Total of 11 GLRLM features namely short run emphasis, long run emphasis, low gray level run emphasis, high gray level run emphasis, short run low gray level emphasis, short run high gray level emphasis, long run low gray level emphasis, long run high gray level emphasis, gray level non uniformity, run length non-uniformity and run percentage are computed from each ROI [47, 48].

3.4.1.4. Other Statistical Features

(*a*) *Edge Features (Absolute Gradient)*: The edges in an image contain more information about the texture than other parts of the image. The gradient of an image can be used to measure the spatial variation of gray levels across an image. At an edge, there is an abrupt change in gray level of the image. If there is an abrupt change in gray level, at some point then the point is said to have a high gradient and if the variation is smooth the point is at low gradient. Absolute gradient is used to judge whether the gray level variation in an image is smooth or abrupt. The texture features computed are absolute gradient mean and absolute gradient variance [49].

(*b*) *Neighborhood Gray Tone Difference Matrix (NGTDM) Features*: NGTDM reflects a grayscale difference between pixels with a certain gray scale and the neighboring pixels. Features extracted from NGTDM are: coarseness, contrast, business, complexity and strength [25, 50].

(*c*) *Statistical Feature Matrix (SFM)*: SFM is used to measure the statistical properties of pixels at several distances within an image. The features computed from SFM are coarseness, contrast, periodicity and roughness.

(*d*) *Gray Level Difference Statistics (GLDS)*: These features are based on the co-occurrence of a pixel pair having a given absolute difference in gray-levels separated by a particular distance. The extracted features are: homogeneity, contrast, energy, entropy and mean [51, 52].

3.4.2. Signal Processing based Methods

Laws' Mask Texture Analysis: In this method small convolution masks are used as filters and ROIs are convolved with these special filters so that the underlying texture characteristics are enhanced. These filters determine the properties of the texture by performing averaging, edge detection, spot detection, wave detection and ripple detection [53-58]. Laws' masks of lengths 3, 5, 7 and 9 are used to compute five statistical parameters i.e. mean, standard deviation, skewness, kurtosis and entropy from each ROI.

3.4.3. Transform Domain based Methods

Feature extraction can also be done in the transform domain over various scales by using different multiresolution schemes like DWT, wavelet packet transform (WPT) and GWT. It is logical to compute texture features in the transform domain as human visual system processes images in a multiscale way and scale is considered to be an important aspect for analysis of texture [59-61].

3.4.3.1. Two Dimensional Discrete Wavelet Transform

A two-dimensional DWT when applied to images can be seen as two one-dimensional transform functions applied to rows and columns of the image separately [61]. When this operation is applied to an ROI image and decomposition is done upto second level, one approximate subimage A_j and six orientation selective detailed subimages $D_j^{(k)}, k = h, v, d$ are generated. This wavelet representation of an image is shown in Figure 3.5. From each subimage, normalized energy is computed as a texture measure.

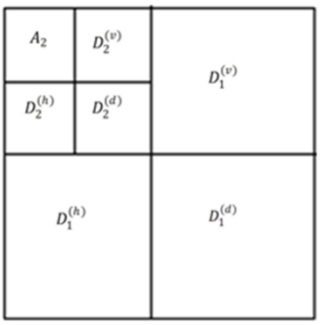

Figure 3.5 Wavelet representation of image up to 2nd level of decomposition.

The choice of wavelet filter used for feature extraction is based on some properties which are significant for texture description [62, 63]. The properties that

are considered for selecting an appropriate wavelet filter include: support width, orthogonality or biorthogonality, shift invariance and symmetry. Wavelet filters that provide compact support are desirable due to their ease of implementation. Orthogonality is required for energy conservation at each level of decomposition. Symmetry is desired to avoid any dephasing while processing images. Based on these properties wavelet filters like Haar (db1), Daubechies (db4 and db6), Coiflets (coif1 and coif2), Symlets (sym3 and sym 5) and Biorthogonal (bior3.1, bior3.3 and bior4.4) are considered for analysis. The properties of these filters are summarized in Table 3.1.

Table 3.1: Properties of wavelet filters used

Wavelet Filter	Biorthogonal	Orthogonal	Symmetry	Asymmetry	Near Symmetry	Compact Support
Db	No	Yes	No	Yes	No	Yes
Haar	No	Yes	Yes	No	No	Yes
Bior	Yes	No	Yes	No	No	Yes
Coif	No	Yes	No	No	Yes	Yes
Sym	No	Yes	No	No	Yes	Yes

3.4.3.2.Two Dimensional Gabor Wavelet Transform

The application of 2D-GWT results in a set of frequency and orientation selective filters that capture energy at a specific frequency and orientation. The 2D-GWT, considering three scales (0,1 and 2) and seven angles (22.5°, 45°, 67.5°, 90°, 112.5°, 135° and 157.5°) result in a group of 21 wavelets (7 × 3). When this group of wavelets is convolved with the ROI image, a set of 21 feature images are obtained. Each of these filtered images represents image information at a certain scale and orientation [63, 64]. From these 21 feature images, mean and standard deviation are computed as texture features forming a texture feature vector (TFV) of length 42. The real part of the 21 wavelets resulting from a 13 × 13 convolution mask with 3 scales and 7 orientations are shown in Figure 3.6.

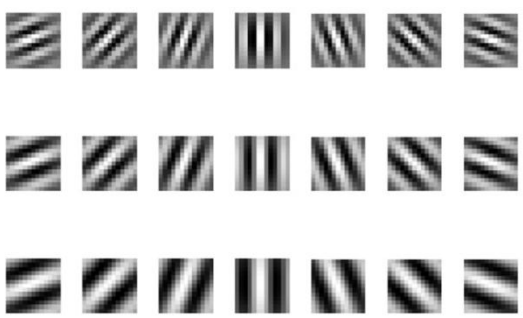

Figure 3.6 Real part of Gabor filter family of 21 wavelets.

3.4.3.3. Fourier Power Spectrum Features

Two spectral features namely radial sum and angular sum are computed from each ROI using discrete Fourier transform.

3.5. Feature Space Dimensionality Reduction Module

The texture feature vector formed after computing the texture features in the feature extraction module may contain some redundant and correlated features which when used in the classification task can degrade the performance of the proposed CAD system. These redundant features give no extra information that proves to be helpful in discriminating the textural changes exhibited by different density patterns. Hence, to remove these redundant features and obtain the optimal attributes for the classification task, PCA is employed [65-67]. Steps used in the PCA algorithm are:

(1) Normalize each feature in dataset to zero mean and unity variance.

(2) Obtain co-variance matrix of the training dataset.

(3) Obtain Eigen values and Eigen vectors from the co-variance matrix. Eigen vectors give the directions of the PCs.

(4) Project the data points in testing dataset in the direction of the PCs of training dataset.

The obtained PCs are uncorrelated to each other and the 1^{st} PC has the largest possible variance out of all the successive PCs. The optimal number of PCs is determined by performing repeated experiments by going through first few PCs i.e. by first considering the first two PCs, then first three PCs and so on, and evaluating the performance of the classifier for each experiment.

3.6. Classification Module

Classification is a machine learning technique used to predict the class membership of unknown data instances based on the training set of data containing instances whose class membership is known. In this module different classifiers like kNN, PNN, SVM and SSVM are employed to classify the unknown testing instances of mammographic images different classes based on the training instances. To avoid any bias caused by unbalanced feature values the extracted features are normalized in the range [0, 1] by using min-max normalization procedure.

3.6.1. k-Nearest Neighbour (kNN) Classifier

The kNN classifier is based on the idea of estimating the class of an unknown instance from its neighbors. It tries to cluster the instances of feature vector into disjoint classes with an assumption that instances of feature vector lying close to each other in feature space represent instances belonging to the same class. The class of an unknown instance in testing dataset is selected to be the class of majority of instances among its *k*-nearest neighbors in the training dataset. The advantage of kNN is its ability to deal with multiple class problems and is robust to noisy data as it averages the *k*- nearest neighbors [67-70]. Euclidean distance is used as a distance metric. The classification performance of kNN classifier depends on the value of *k*. In the present work, the optimal value of *k* and number of PCs to be retained is determined by performing repeated experiments for the values of $k \in \{1,2,\dots,9,10\}$ and number of PCs $\in \{1,2,\dots\dots 14,15\}$. If same accuracy is obtained for more than one value of *k*, smallest value of *k* is used to obtain the result. The example depicting the classification of an unknown instance is shown in Figure 3.7. In the example the test sample (×) should be either classified to the class of cross (+) or to the class of dash (-). When $k = 3$, the algorithm looks for three nearest neighbors. In the considered example, the test sample is assigned to the class of cross (+) because there are two cross and only one dash inside the circle.

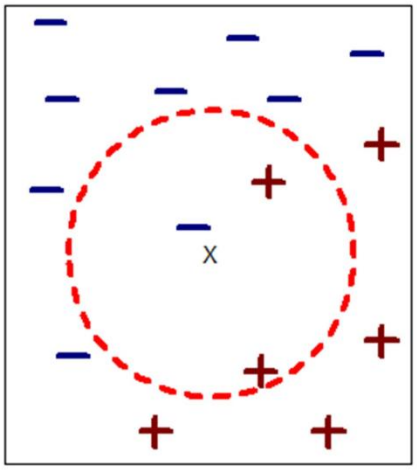

Figure 3.7 Example of kNN classification for $k = 3$.
Note: ×: unknown instance, +: Instance of class 1, –: Instance of class 2.

3.6.2. Probabilistic Neural Network (PNN) Classifier

The PNN is a supervised feed-forward neural network used for estimating the probability of class membership [67, 71-73]. The architecture of PNN consists of four layers: input layer, pattern layer, summation layer and output layer. Primitive values are passed to the '*n*' neurons in the input unit. Values from the input unit are passed to the hidden units in the pattern layer where responses for each unit are calculated. There are '*k*' number of neurons in the pattern layer, one for each class. In the pattern layer a probability density function for each class is defined based on the training dataset and optimized kernel width parameter. Values of each hidden unit are summed in the summation layer to get response in each category. Maximum response is taken from all categories in the decision layer to get the class of the unknown instance. The optimal choice of spread parameter (Sp) i.e. the kernel width parameter is critical for the classification using PNN. In the present work the optimal values used for Sp and optimal number of PCs to design a PNN classifier are determined by performing repeated experiments for values of $\mathrm{Sp} \in \{1,2, \ldots 9,10\}$ and number of $\mathrm{PCs} \in \{1,2, \ldots 14, 15\}$.

3.6.3. Support Vector Machine (SVM) Classifier

The SVM classifier belongs to a class of supervised machine learning algorithms. It is based on the concept of decision planes that define the decision boundary. In SVM, kernel functions are used to map the non-linear training data from input space to a high dimensionality feature space. Some common kernels are polynomial, Gaussian radial basis function and sigmoid. In the present work SVM classifier is implemented using LibSVM library [74] and the performance of the Gaussian Radial Basis Function kernel is investigated. The critical step for obtaining a good generalization performance is the correct choice of regularization parameter C and kernel parameter γ. The regularization parameter C tries to maximize the margin while keeping the training error low. In the present work, ten-fold cross validation is carried out on the training data, for each combination of (C, γ) such that, $\mathrm{C} \in \{2^{-4}, 2^{-3} \ldots 2^{15}\}$ and $\gamma \in \{2^{-12}, 2^{-11} \ldots 2^{4}\}$. This grid search procedure in parameter space gives the optimum values of C and γ for which training accuracy is maximum [66, 67, 75-77].

3.6.4. Smooth Support Vector Machine (SSVM) Classifier

To solve important mathematical problems related to programming, smoothing methods are extensively used. SSVM works on the idea of smooth unconstrained optimization reformulation based on the traditional quadratic program which is associated with SVM [78, 79]. For implementing SSVM classifier, the SSVM toolbox developed by Laboratory of Data Science and Machine Intelligence, Taiwan was used [80]. Similar to SVM implementation in case of SSVM also, ten-fold cross validation is carried out on training data for each combination of (C, γ), $C \in \{2^{-4}, 2^{-3} \ldots 2^{15}\}$ and $\gamma \in \{2^{-12}, 2^{-11} \ldots 2^{4}\}$. This grid search procedure in parameter space gives the optimum values of C and γ for which training accuracy is maximum.

3.7. Concluding Remarks

After carrying out extensive literature survey, it was observed that various CAD system designs have proven useful to the radiologists in routine medical practice as second opinion tools for breast tissue density classification of mammograms in cases where a clear discrimination cannot be made subjectively between the overlapping density patterns. In light of this fact, different CAD system designs employing the texture analysis techniques of feature extraction, feature space dimensionality reduction and feature classification have been proposed in the present work for two-class and three-class breast tissue density classification of mammograms. Feature extraction is done using statistical, signal processing based and transforms domain based methods. To reduce the redundant features, PCA has been employed and finally classification performance of each TFV is evaluated using different classifiers.

A detailed description of each CAD system design is given in the forthcoming chapters.

Chapter 4

CAD System Design for Breast Tissue Density Classification Using Statistical Features

4.1. Introduction

The differential diagnosis between atypical breast tissue density patterns from mammographic images is a daunting challenge even for the experienced radiologists due to overlap of the appearances of the density patterns. Therefore a CAD system for the classification of the different breast tissue density patterns from mammographic images is highly desirable. In light of this fact, a CAD system design is proposed in this chapter to evaluate the performance of different classifiers for two-class and three-class breast tissue density classification.

4.2. Proposed CAD System Design

The block diagram of the proposed CAD system design for two-class and three-class breast tissue density classification using statistical features is shown in Figure 4.1. The approach is implemented on the 322 mammograms of the MIAS database. From each mammographic image, ROIs of size 200 × 200 are extracted and from each ROI image, different statistical features are calculated like FOS, GLCM features, GLRL features, features derived from GLDS, NGTDM features, SFM features and Edge features.

To the resultant texture feature vector (TFV), PCA is applied to calculate the optimal number of PCs required for the classification task forming a reduced texture feature vector (RTFV). The classification problem is divided into two parts. In the first part, the mammograms are classified into two categories namely fatty and dense. In the second part of the classification problem, the mammograms are classified into three categories namely fatty, fatty-glandular and dense-glandular.

4.3. Experimental Workflow and Results

For evaluating the performance of the proposed CAD system design, rigorous experimentation has been carried out for the characterization of the breast tissue based on its density. A brief description of experiments is given in Table 4.1 and Table 4.2, respectively for two-class and three-class breast tissue density classification.

Table 4.1: Description of experiments carried out for two-class breast tissue density classification

Experiment 1:	To obtain the classification performance of statistical features for two-class breast tissue density classification using kNN, PNN, SVM and SSVM classifiers.
Experiment 2:	To obtain the classification performance of statistical features for two-class breast tissue density classification using PCA-kNN, PCA-PNN, PCA-SVM and PCA-SSVM classifiers.

Table 4.2: Description of experiments carried out for three-class breast tissue density classification

Experiment 1:	To obtain the classification performance of statistical features for three-class breast tissue density classification using kNN, PNN, SVM and SSVM classifiers.
Experiment 2:	To obtain the classification performance of statistical features for three-class breast tissue density classification using PCA-kNN, PCA-PNN, PCA-SVM and PCA-SSVM classifiers.

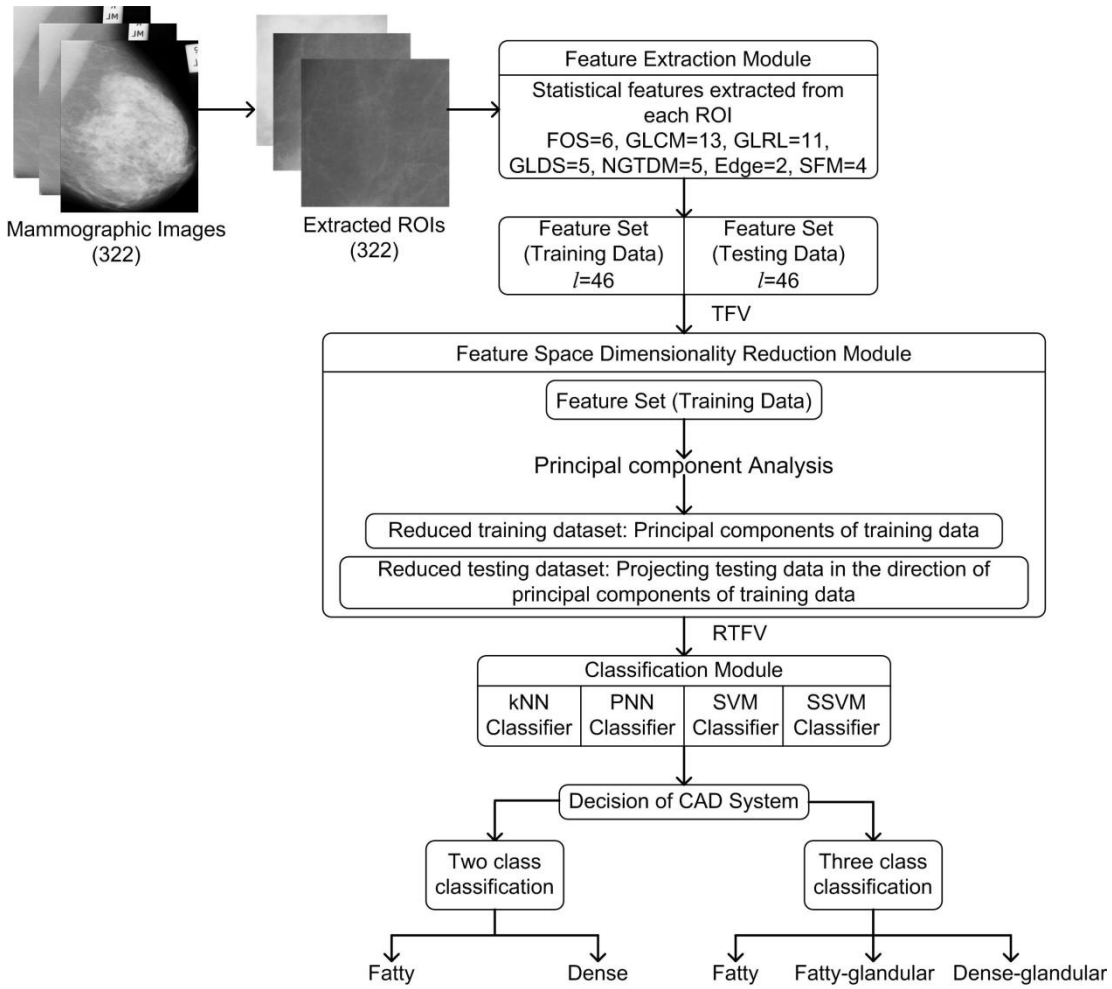

Figure 4.1 Proposed CAD system design using statistical features for two-class and three-class breast tissue density classification.

4.3.1. Experiments carried out for two-class breast tissue density classification

4.3.1.1. Experiment 1: To obtain the classification performance of statistical features for two-class breast tissue density classification using kNN, PNN, SVM and SSVM classifiers.

In this experiment, classification performance of TFV containing different statistical features is evaluated for two-class breast tissue density classification using different classifiers. The results of the experiment are shown in Table 4.3. It can be observed from the table that for statistical features, the overall classification accuracy of 92.5 %, 91.3 %, 90.6 % and 92.5 % is achieved using kNN, PNN, SVM and SSVM classifiers, respectively. It can also be observed that the highest in individual class accuracy for fatty class is 83.0 % with SSVM classifier and highest individual class accuracy for dense class is 100.0 %, using PNN classifier. Out of total 161 testing instances, 12 instances (12/161) are misclassified in case of kNN, 14 instances (14/161) are misclassified in case of PNN, 16 instances (16/161) are misclassified in case of SVM and 12 instances (12/161) are misclassified in case of SSVM classifier.

Table 4.3: Classification performance of statistical features using kNN, PNN, SVM and SSVM classifiers for two-class breast tissue density classification

Classifier	CM			OCA (%)	ICA_F (%)	ICA_D (%)
kNN		F	D	92.5	81.1	98.1
	F	43	10			
	D	2	106			
PNN	F	39	14	91.3	73.5	100.0
	D	0	108			
SVM	F	41	12	90.6	77.3	96.2
	D	4	104			
SSVM	F	44	9	92.5	83.0	97.2
	D	3	105			

Note: CM: Confusion matrix, F: Fatty class, D: Dense class, OCA: Overall classification accuracy; ICA_F: Individual class accuracy for fatty class. ICA_D: Individual class accuracy for dense class.

4.3.1.2. Experiment 2: To obtain the classification performance of statistical features for two-class breast tissue density classification using PCA-kNN, PCA-PNN, PCA-SVM and PCA-SSVM classifiers.

In this experiment, classification performance of TFV containing different statistical features is evaluated for two-class breast tissue density classification using different classifiers. The results are shown in Table 4.4. It can be observed from the table that the overall classification values of 91.9 %, 91.3 %, 93.7 % and 94.4 % have been achieved using the PCA-kNN, PCA-PNN, PCA-SVM and PCA-SSVM classifiers, respectively.

Table 4.4: Classification performance of statistical features using PCA-kNN, PCA-PNN, PCA-SVM and PCA-SSVM classifiers for two-class breast tissue density classification

Classifier	*l*	CM			OCA (%)	ICA_F (%)	ICA_D (%)
kNN	6		F	D	91.9	81.1	97.2
		F	43	10			
		D	3	105			
PNN	4	F	39	14	91.3	73.5	100.0
		D	0	108			
SVM	7	F	43	10	93.7	81.1	100.0
		D	0	108			
SSVM	10	F	47	6	94.4	88.6	97.2
		D	3	105			

Note: *l*: No. of PCs, CM: Confusion matrix, F: Fatty class, D: Dense class, OCA: Overall classification accuracy; ICA_F: Individual class accuracy for fatty class. ICA_D: Individual class accuracy for dense class.

It can also be observed that the highest individual class accuracy for fatty class is 88.6 % using PCA-SSVM classifier and that for dense class is 100.0 % using PCA-PNN and PCA-SVM classifiers. Out of total 161 testing instances, 13 instances (13/161) are misclassified in case of PCA-kNN, 14 instances (14/161) are misclassified in case of PCA-PNN, 10 instances (10/161) are misclassified in case of PCA-SVM and 9 instances (9/161) are misclassified in case of PCA-SSVM classifier.

4.3.2. Experiments carried out for three-class breast tissue density classification

4.3.2.1. Experiment 1: To obtain the classification performance of statistical features for three-class breast tissue density classification using kNN, PNN, SVM and SSVM classifiers.

In this experiment, the classification performance of TFV containing different statistical features is evaluated for three-class breast tissue density classification using different classifiers. The results are shown in Table 4.5. It can be observed from the table that the overall classification accuracy of 86.9 %, 85.0 %, 83.8 % and 82.6 % is achieved using kNN, PNN, SVM and SSVM classifiers, respectively. The highest individual class accuracy for fatty class is 94.3 % using SVM classifier, for fatty-glandular class the highest individual class accuracy achieved is 88.4 % using SSVM classifier and for the dense-glandular class, highest individual class accuracy achieved is 96.4 % using kNN classifier. Out of total 161 testing instances, 21 instances (21/161) are misclassified in case of kNN, 24 instances (24/161) are misclassified in case of PNN, 26 instances (26/161) are misclassified in case of SVM and 28 instances (28/161) are misclassified in case of SSVM classifier.

Table 4.5: Classification performance of statistical features using kNN, PNN, SVM and SSVM classifiers for three-class breast tissue density classification

Classifier	CM				OCA (%)	ICA_F (%)	ICA_{FG} (%)	ICA_{DG} (%)
kNN		F	FG	DG	86.9	86.7	76.9	96.4
	F	46	2	5				
	FG	2	40	10				
	DG	0	2	54				
PNN	F	41	8	4	85.0	77.3	82.6	94.6
	FG	1	43	8				
	DG	0	3	53				
SVM	F	50	3	0	83.8	94.3	67.3	89.2
	FG	12	35	5				
	DG	1	5	50				
SSVM	F	39	11	3	82.6	73.5	88.4	85.7
	FG	3	46	3				
	DG	1	7	48				

Note: CM: Confusion matrix, F: Fatty class, FG: Fatty–glandular class, DG: Dense-glandular class, OCA: Overall classification accuracy; ICA_F: Individual class accuracy for fatty class, $ICA_{FG:}$ Individual class accuracy for fatty-glandular class, ICA_{DG}: Individual class accuracy for dense-glandular class.

4.3.2.2. Experiment 2: To obtain the classification performance of statistical features for three-class breast tissue density classification using PCA-kNN, PCA-PNN, PCA-SVM and PCA-SSVM classifiers.

In this experiment, the classification performance of TFV containing different statistical features is evaluated for three-class breast tissue density classification using different classifiers. The results are shown in Table 4.6.

Table 4.6: Classification performance of statistical features using PCA-kNN, PCA-PNN, PCA-SVM and PCA-SSVM classifiers for three-class breast tissue density classification

Classifier	*l*	CM				OCA (%)	ICA_F (%)	ICA_{FG} (%)	ICA_{DG} (%)
kNN	9		F	FG	DG	85.0	83.0	73.0	98.2
		F	44	4	5				
		FG	3	38	11				
		DG	1	0	55				
PNN	6	F	43	6	4	84.4	81.1	84.6	87.5
		FG	1	44	7				
		DG	0	7	49				
SVM	4	F	47	4	2	86.3	88.6	76.9	92.8
		FG	6	40	6				
		DG	0	4	52				
SSVM	5	F	43	9	1	85.0	81.1	84.6	89.2
		FG	4	44	4				
		DG	0	6	50				

Note: *l*: Optimal number of PCs, CM: Confusion matrix, F: Fatty class, FG: Fatty–glandular class, DG: Dense-glandular class, OCA: Overall classification accuracy; ICA_F: Individual class accuracy for fatty class, $ICA_{FG:}$ Individual class accuracy for fatty-glandular class, ICA_{DG}: Individual class accuracy for dense-glandular class.

It can be observed from the table that the overall classification of 85.0 %, 84.4 %, 86.3 % and 85.0 % is achieved using PCA-kNN, PCA-PNN, PCA-SVM and PCA-SSVM classifiers, respectively. The highest individual class accuracy for fatty class is 88.6 % using PCA-SVM classifier, for fatty-glandular class the highest individual class accuracy achieved is 84.6 % using PCA-PNN and PCA-SSVM classifiers and for the dense-glandular class, highest individual class accuracy achieved is 98.2 % using PCA-kNN classifier. Out of total 161 testing instances, 24 instances (24/161) are misclassified in case of PCA-kNN, 25 instances (25/161) are misclassified in case of PCA-PNN, 22 instances (22/161) are misclassified in case of PCA-SVM and 24 instances (24/161) are misclassified in case of PCA-SSVM classifier.

4.4. Concluding Remarks

From the results obtained from the above experiments, it can be observed that for two-class breast tissue density, PCA-SSVM classifier achieves highest classification accuracy of 94.4 % using first 10 PCs thus, it can be concluded that for two-class breast tissue density classification, first 10 PCs obtained by applying PCA to the TFV derived using statistical features are sufficient to account for the textural changes exhibited by the fatty and dense breast tissue.

For three-class breast tissue density classification, it can be observed from the above experiments that highest classification accuracy of 86.9 % is achieved using the kNN classifier, however it should also be noted that PCA-SVM classifier achieves the highest classification accuracy of 86.3 % by using only the first 4 PCs obtained by applying PCA to the TFV of statistical features. Thus CAD system design based on PCA-SVM classifier can be considered to be the best choice for three-class breast tissue density classification.

Chapter 5

CAD System Design for Breast Tissue Density Classification Using Laws' Texture Features

5.1. Introduction

Characterization of tissue density is clinically significant as high density is associated with the risk of developing breast cancer and also masks lesions. It is believed that the changes in the tissue density can be captured by computing the texture features. Accordingly, the objective of the present chapter is to explore Laws' mask analysis for description of variations in breast tissue density using mammographic images for two-class and three-class breast tissue density classification.

5.2. Proposed CAD System Design

The block diagram of the proposed CAD system design for two-class and three-class breast tissue density using Laws' texture features is shown in Figure 5.1.

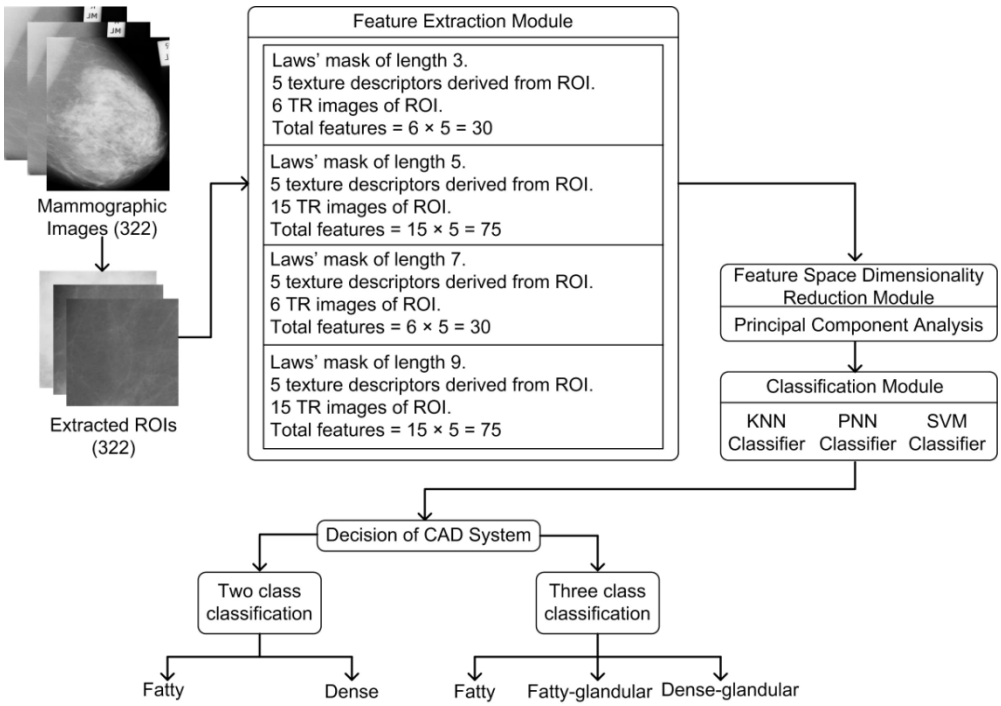

Figure 5.1 Proposed CAD system design using Laws' texture features for two-class and three-class breast tissue density classification.

For the design of the proposed CAD system, Laws' texture features have been computed using Laws' masks of different resolutions i.e., Laws' mask of length 3, 5, 7 and 9. The feature space dimensionality reduction has been carried out by using

PCA. For the classification task, kNN, PNN and SVM classifiers have been used for two-class and three-class breast tissue density classification. The description of the TFVs derived from Laws' masks of different resolutions is given in Table 5.1.

Table 5.1: Description of texture feature vectors

TFV1:	TFV derived from Laws' mask of length 3 (5 statistical features computed from 6 TR images)
TFV2:	TFV derived from Laws' mask of length 5 (5 statistical features computed from 15 TR images)
TFV3:	TFV derived from Laws' mask of length 7 (5 statistical features computed from 6 TR images)
TFV4:	TFV derived from Laws' mask of length 9 (5 statistical features computed from 15 TR images)
RTFV1:	Reduced TFV consisting of optimal PCs obtained by applying PCA to TFV1
RTFV2:	Reduced TFV consisting of optimal PCs obtained by applying PCA to TFV2
RTFV3:	Reduced TFV consisting of optimal PCs obtained by applying PCA to TFV3
RTFV4:	Reduced TFV consisting of optimal PCs obtained by applying PCA to TFV4

Note: TFV: Texture feature vector, TR: Rotation invariant images, RTFV: Reduced texture feature vector.

5.3. Experimental Workflow and Results

For evaluating the performance of the proposed CAD system design, various experiments have been carried out to characterize the breast tissue for two-class and three-class breast tissue density classification. A brief description of the conducted experiments for two-class and three-class breast tissue density classification is tabulated in Table 5.2 and Table 5.3, respectively.

Table 5.2: Description of experiments carried out for two-class breast tissue density classification

Experiment 1	To obtain classification performance of different TFVs (derived from Laws' masks of length 3, 5, 7 and 9) using kNN classifier
Experiment 2	To obtain classification performance of different TFVs (derived from Laws' masks of length 3, 5, 7 and 9) using PNN classifier
Experiment 3	To obtain classification performance of different TFVs (derived from Laws' masks of length 3, 5, 7 and 9) using SVM classifier
Experiment 4	To obtain classification performance of different RTFVs (derived from Laws' masks of length 3, 5, 7 and 9) using PCA-kNN classifier
Experiment 5	To obtain classification performance of different RTFVs (derived from Laws' masks of length 3, 5, 7 and 9) using PCA-PNN classifier
Experiment 6	To obtain classification performance of different RTFVs (derived from Laws' masks of length 3, 5, 7 and 9) using PCA-SVM classifier

Note: TFV: Texture feature vector. RTFV: Reduced texture feature vector.

Table 5.3: Description of experiments carried for three-class breast tissue density classification

Experiment 1	To obtain classification performance of different TFVs (derived from Laws' masks of length 3, 5, 7 and 9) using kNN classifier
Experiment 2	To obtain classification performance of different TFVs (derived from Laws' masks of length 3, 5, 7 and 9) using PNN classifier
Experiment 3	To obtain classification performance of different TFVs (derived from Laws' masks of length 3, 5, 7 and 9) using SVM classifier
Experiment 4	To obtain classification performance of different RTFVs (derived from Laws' masks of length 3, 5, 7 and 9) using PCA-kNN classifier
Experiment 5	To obtain classification performance of different RTFVs (derived from Laws' masks of length 3, 5, 7 and 9) using PCA-PNN classifier
Experiment 6	To obtain classification performance of different RTFVs (derived from Laws' masks of length 3, 5, 7 and 9) using PCA-SVM classifier

Note: TFV: Texture feature vector. RTFV: Reduced texture feature vector.

5.3.1. Experiments carried out for two-class breast tissue density classification

5.3.1.1. Experiment 1: To obtain classification performance of different TFVs (derived from Laws' masks of length 3, 5, 7 and 9) using kNN classifier.

In this experiment the classification performance of the feature set containing instances of TFV1, TFV2, TFV3 and TFV4 is evaluated using kNN classifier. The results are shown in Table 5.4.

Table 5.4: Classification performance of different TFVs using kNN classifier for two-class breast tissue density classification

TFV(*l*)	CM			OCA (%)	ICA_F (%)	ICA_D (%)
TFV1(30)		F	D	93.1	81.1	99.0
	F	43	10			
	D	1	107			
TFV2(75)	F	44	9	92.5	83.0	97.2
	D	3	105			
TFV3(30)	F	46	7	95.0	86.7	99.0
	D	1	107			
TFV4(75)	F	42	11	90.6	79.2	96.2
	D	4	104			

Note: TFV: Texture feature vector, *l*: Length of TFV, CM: Confusion Matrix, F: Fatty class, D: Dense class, OCA: Overall classification accuracy; ICA_F: Individual class accuracy for fatty class. ICA_D: Individual class accuracy for dense class.

From the table it can be observed that a classification accuracy of 93.1 %, 92.5 %, 95.0 % and 90.6 % is achieved using TFV1, TFV2, TFV3 and TFV4, respectively. The individual class accuracy of fatty class is 81.1 %, 83.0 %, 86.7 % and 79.2 % for TFV1, TFV2, TFV3 and TFV4, respectively. For dense class the individual class accuracy is 99.0 %, 97.2 %, 99.0 % and 96.2 % for TFV1, TFV2, TFV3 and TFV4, respectively. Out of 161 instances of testing data, 11 instances (11/161) are misclassified in case of TFV1, 12 instances (12/161) are misclassified in

case of TFV2, 8 instances (8/161) are misclassified in case of TFV3 and 15 instances (15/161) are misclassified in case of TFV4.

5.3.1.2. Experiment 2: To obtain classification performance of different TFVs (derived from Laws' masks of length 3, 5, 7 and 9) using PNN classifier.

In this experiment the classification performance of the feature set containing instances of TFV1, TFV2, TFV3 and TFV4 is evaluated using PNN classifier. The results are shown in Table 5.5.

Table 5.5: Classification performance different TFVs using PNN classifier for two-class breast tissue density classification

TFV(*l*)	**CM**			**OCA (%)**	**ICA_F (%)**	**ICA_D (%)**
TFV1(30)		F	D	91.3	79.2	97.2
	F	42	11			
	D	3	105			
TFV2(75)	F	46	7	91.9	86.7	94.4
	D	6	102			
TFV3(30)	F	43	10	91.9	81.1	97.2
	D	3	105			
TFV4(75)	F	43	10	88.8	81.1	92.5
	D	8	100			

Note: TFV: Texture feature vector, *l*: Length of TFV, CM: Confusion Matrix, F: Fatty class, D: Dense class, OCA: Overall classification accuracy; ICA_F: Individual class accuracy for fatty class. ICA_D: Individual class accuracy for dense class.

From the table it can be observed that a classification accuracy of 91.3 %, 91.9 %, 91.9 % and 88.8 % is achieved using TFV1, TFV2, TFV3 and TFV4, respectively. The individual class accuracy for fatty class is 79.2 %, 86.7 %, 81.1 % and 81.1 % for TFV1, TFV2, TFV3 and TFV4, respectively. For dense class the individual class accuracy is 97.2 %, 94.4 %, 97.2 % and 92.5 % for TFV1, TFV2, TFV3 and TFV4, respectively. Out of 161 instances of testing data, 14 instances (14/161) are misclassified in case of TFV1, 13 instances (13/161) are misclassified in case of TFV2, 13 instances (13/161) are misclassified in case of TFV3 and 18 instances (18/161) are misclassified in case of TFV4.

5.3.1.3. Experiment 3: To obtain classification performance of different TFVs (derived from Laws' masks of length 3, 5, 7 and 9) using SVM classifier

In this experiment the classification performance of the feature set containing instances of TFV1, TFV2, TFV3 and TFV4 is evaluated using the SVM classifier. The results are shown in Table 5.6. From the table it can be observed that a classification accuracy of 91.3 %, 93.1 %, 91.9 % and 92.5 %, is achieved using

TFV1, TFV2, TFV3 and TFV4, respectively. The individual class accuracy for fatty class is 81.1 %, 81.1 %, 81.1 % and 83.0 % for TFV1, TFV2, TFV3 and TFV4, respectively. For dense class the individual class accuracy is 96.2 %, 99.0 %, 97.2 % and 97.2 % for TFV1, TFV2, TFV3 and TFV4, respectively. Out of 161 instances of testing data, 14 instances (14/161) are misclassified in case of TFV1, 11 instances (11/161) are misclassified in case of TFV2, 13 instances (13/161) are misclassified in case of TFV3 and 12 instances (12/161) are misclassified in case of TFV4.

Table 5.6: Classification performance of different TFVs using SVM classifier for two-class breast tissue density classification

TFV(*l*)	**CM**			**OCA (%)**	**ICA_F (%)**	**ICA_D (%)**
TFV1(30)		F	D	91.3	81.1	96.2
	F	43	10			
	D	4	104			
TFV2(75)	F	43	10	93.1	81.1	99.0
	D	1	107			
TFV3(30)	F	43	10	91.9	81.1	97.2
	D	3	105			
TFV4(75)	F	44	9	92.5	83.0	97.2
	D	3	105			

Note: TFV: Texture feature vector, *l*: Length of TFV, CM: Confusion Matrix, F: Fatty class, D: Dense class, OCA: Overall classification accuracy; ICA_F: Individual class accuracy for fatty class. ICA_D: Individual class accuracy for dense class.

5.3.1.4. Experiment 4: To obtain classification performance of different RTFVs (derived from Laws' masks of length 3, 5, 7 and 9) using PCA-kNN classifier.

In this experiment the classification performance of the feature set containing instances of RTFV1, RTFV2, RTFV3 and RTFV4 is evaluated using PCA-kNN classifier. The results are shown in Table 5.7. From the table it can be observed that a classification accuracy of 92.5 %, 95.6 %, 94.4 % and 92.5 % is achieved using RTFV1, RTFV2, RTFV3 and RTFV4. The RTFV1, RTFV2, RTFV3 and RTFV4 are reduced forms of TFV1, TFV2, TFV3 and TFV4 obtained after applying PCA. The individual class accuracy for fatty class is 83.0 %, 86.7 %, 83.0 % and 83.0 % for RTFV1, RTFV2, RTFV3 and RTFV4, respectively. For dense class the individual class accuracy is 97.2 %, 100.0 %, 100.0 % and 97.2 % for RTFV1, RTFV2, RTFV3 and RTFV4, respectively. Out of 161 instances of testing data, 12 instances (12/161) are misclassified in case of RTFV1, 7 instances (7/161) are misclassified in case of RTFV2, 9 instances (9/161) are misclassified in case of RTFV3 and 12 instances (12/161) are misclassified in case of RTFV4.

Table 5.7: Classification performance of different RTFVs using PCA-kNN classifier for two-class breast tissue density classification

TFV(*l*)	CM			OCA (%)	ICA_F (%)	ICA_D (%)
RTFV1(5)		F	D	92.5	83.0	97.2
	F	44	9			
	D	3	105			
RTFV2(8)	F	46	7	95.6	86.7	100.0
	D	0	108			
RTFV3(4)	F	44	9	94.4	83.0	100.0
	D	0	108			
RTFV4(10)	F	44	9	92.5	83.0	97.2
	D	3	105			

Note: RTFV: Reduced texture feature vector, *l*: Optimum number of PCs, CM: Confusion Matrix, F: Fatty class, D: Dense class, OCA: Overall classification accuracy; ICA_F: Individual class accuracy for fatty class. ICA_D: Individual class accuracy for dense class.

5.3.1.5. Experiment 5: To obtain the classification performance of different RTFVs (derived from Laws' masks of length 3, 5, 7 and 9) using PCA-PNN classifier.

In this experiment the classification performance of the feature set containing instances of RTFV1, RTFV2, RTFV3 and RTFV4 is evaluated using the PCA-PNN classifier. The results are shown in Table 5.8.

Table 5.8: Classification performance of different RTFVs using PCA-PNN classifier for two-class breast tissue density classification

TFV(*l*)	CM			OCA (%)	ICA_F (%)	ICA_D (%)
RTFV1(5)		F	D	92.5	83.0	97.2
	F	44	9			
	D	3	105			
RTFV2(4)	F	37	16	89.4	69.8	99.0
	D	1	107			
RTFV3(4)	F	43	10	92.5	81.1	98.1
	D	2	106			
RTFV4(4)	F	37	16	89.4	69.8	99.0
	D	1	107			

Note: RTFV: Reduced texture feature vector, *l*: Optimum number of PCs, CM: Confusion Matrix, F: Fatty class, D: Dense class, OCA: Overall classification accuracy; ICA_F: Individual class accuracy for fatty class. ICA_D: Individual class accuracy for dense class.

From the table it can be observed that a classification accuracy of 92.5 %, 89.4 %, 92.5 % and 89.4 %, is achieved using RTFV1, RTFV2, RTFV3 and RTFV4, respectively. The RTFV1, RTFV2, RTFV3 and RTFV4 are reduced forms of TFV1, TFV2, TFV3 and TFV4 obtained after applying PCA. The individual class accuracy for fatty class is 83.0 %, 69.8 %, 81.1 % and 69.8 % for RTFV1, RTFV2, RTFV3 and RTFV4, respectively. For dense class the individual class accuracy is 97.2 %, 99.0 %, 98.1 % and 99.0 % for RTFV1, RTFV2, RTFV3 and RTFV4, respectively. Out of 161

instances of testing data, 12 instances (12/161) are misclassified in case of RTFV1, 17 instances (17/161) are misclassified in case of RTFV2, 12 instances (12/161) are misclassified in case of RTFV3 and 17 instances (17/161) are misclassified in case of RTFV4.

5.3.1.6. Experiment 6: To obtain classification performance of different RTFVs (derived from Laws' masks of length 3, 5, 7 and 9) using PCA-SVM classifier.

In this experiment the classification performance of the feature set containing instances of RTFV1, RTFV2, RTFV3 and RTFV4 is evaluated using the PCA-SVM classifier. The results are shown in Table 5.9.

Table 5.9: Classification performance of different RTFVs using PCA-SVM classifier for two-class breast tissue density classification

TFV(*l*)	CM			OCA (%)	ICA_F (%)	ICA_D (%)
RTFV1(5)		F	D	92.5	81.1	98.1
	F	43	10			
	D	2	106			
RTFV2(4)	F	45	8	94.4	84.9	99.0
	D	1	107			
RTFV3(5)	F	44	9	93.1	83.0	98.1
	D	2	106			
RTFV4(4)	F	45	8	91.9	84.9	95.3
	D	5	103			

Note: RTFV: Reduced texture feature vector, *l*: Optimum number of PCs, CM: Confusion Matrix, F: Fatty class, D: Dense class, OCA: Overall classification accuracy; ICA_F: Individual class accuracy for fatty class. ICA_D: Individual class accuracy for dense class.

From the table it can be observed that a classification accuracy of 92.5 %, 94.4 %, 93.1 % and 91.9 %, is achieved using RTFV1, RTFV2, RTFV3 and RTFV4, respectively. The RTFV1, RTFV2, RTFV3 and RTFV4 are reduced forms of TFV1, TFV2, TFV3 and TFV4 obtained after applying PCA. The individual class accuracy for fatty class is 81.1 %, 84.9 %, 83.0 % and 84.9 % for RTFV1, RTFV2, RTFV3 and RTFV4, respectively. For dense class the individual class accuracy is 98.1 %, 99.0 %, 98.1 % and 95.3 % for RTFV1, RTFV2, RTFV3 and RTFV4, respectively. Out of 161 instances of testing data, 12 instances (12/161) are misclassified in case of RTFV1, 9 instances (9/161) are misclassified in case of RTFV2, 11 instances (11/161) are misclassified in case of RTFV3 and 13 instances (13/161) are misclassified in case of RTFV4.

5.3.2. Experiments carried out for three-class breast tissue density classification

5.3.2.1. Experiment 1: To obtain classification performance of different TFVs (derived from Laws' masks of length 3, 5, 7 and 9) using kNN classifier.

In this experiment the classification performance of the feature set containing instances of TFV1, TFV2, TFV3 and TFV4 is evaluated using kNN. The results are shown in Table 5.10.

Table 5.10: Classification performance of different TFVs using kNN classifier for three-class breast tissue density classification

TFV (*l*)	**CM**				**OCA (%)**	**ICA_F (%)**	**ICA_{FG} (%)**	**ICA_{DG} (%)**
TFV1(30)		F	FG	DG	83.2	83.0	82.6	83.9
	F	44	6	3				
	FG	4	43	5				
	DG	0	9	47				
TFV2(75)	F	43	9	1	83.8	81.1	84.6	85.7
	FG	4	44	4				
	DG	0	8	48				
TFV3(30)	F	46	5	2	86.9	86.7	84.6	89.2
	FG	3	44	5				
	DG	0	6	50				
TFV4(75)	F	39	11	3	78.8	73.5	82.6	80.3
	FG	3	43	6				
	DG	2	9	45				

Note: TFV: Texture feature vector, *l*: Length of TFV, CM: Confusion Matrix, F: Fatty class, FG: Fatty-glandular class DG: Dense-glandular class, OCA: Overall classification accuracy; ICA_F: Individual class accuracy for fatty class. ICA_{FG}: Individual class accuracy for fatty-glandular class. ICA_{DG}: Individual class accuracy for dense-glandular class.

From the table it can be observed that a classification accuracy of 83.2 %, 83.8 %, 86.9 % and 78.8 %, is achieved using TFV1, TFV2, TFV3 and TFV4, respectively. The individual class accuracy of fatty class is 83.0 %, 81.1 % 86.7 % and 73.5 % for TFV1, TFV2, TFV3 and TFV4, respectively. For fatty-glandular class, the individual class accuracy is 82.6 %, 84.6 %, 84.6 % and 82.6 % for TFV1, TFV2, TFV3 and TFV4, respectively. For the dense-glandular class the individual class accuracy is 83.9 %, 85.7 %, 89.2 % and 80.3 % for TFV1, TFV2, TFV3 and TFV4, respectively.

Out of 161 instances of testing data, 27 instances (27/161) are misclassified in case of TFV1, 26 instances (26/161) are misclassified in case of TFV2, 21 instances (21/161) are misclassified in case of TFV3 and 34 instances (34/161) are misclassified in case of TFV4.

5.3.2.2. Experiment 2: To obtain classification performance of different TFV (derived from Laws' masks of length 3, 5, 7 and 9) using PNN classifier.

In this experiment the classification performance of the feature set containing instances of TFV1, TFV2, TFV3 and TFV4 is evaluated using the PNN classifier. The results are shown in Table 5.11.

Table 5.11: Classification performance of different TFVs using PNN classifier for three-class breast tissue density classification

TFV(*l*)	**CM**				**OCA (%)**	**ICA_F (%)**	**ICA_{FG} (%)**	**ICA_{DG} (%)**
TFV1(30)		F	FG	DG	85.0	84.9	90.3	80.3
	F	45	6	2				
	FG	3	47	2				
	DG	2	9	45				
TFV2(75)	F	44	9	0	81.9	83.0	84.6	78.5
	FG	7	44	1				
	DG	3	9	44				
TFV3(30)	F	45	7	1	83.8	84.9	88.4	78.5
	FG	5	46	2				
	DG	2	10	44				
TFV4(75)	F	40	13	0	78.2	75.4	88.4	71.4
	FG	5	46	1				
	DG	6	10	40				

Note: TFV: Texture feature vector, *l*: Length of TFV, CM: Confusion Matrix, F: Fatty class, FG: Fatty-glandular class DG: Dense-glandular class, OCA: Overall classification accuracy; ICA_F: Individual class accuracy for fatty class. ICA_{FG}: Individual class accuracy for fatty-glandular class. ICA_{DG}: Individual class accuracy for dense-glandular class.

From the table it can be observed that a classification accuracy of 85.0 %, 81.9 %, 83.8 % and 78.2 %, is achieved using TFV1, TFV2, TFV3 and TFV4, respectively. The individual class accuracy of fatty class is 84.9 %, 83.0 % 84.9 % and 75.4 % for TFV1, TFV2, TFV3 and TFV4, respectively. For fatty-glandular class, the individual class accuracy is 90.3 %, 84.6 %, 88.4 % and 88.4 % for TFV1, TFV2, TFV3 and TFV4, respectively. For the dense-glandular class the individual class accuracy is 80.3 %, 78.5 %, 78.5 % and 71.4 % for TFV1, TFV2, TFV3 and TFV4, respectively.

Out of 161 instances of testing data, 24 instances (24/161) are misclassified in case of TFV1, 29 instances (29/161) are misclassified in case of TFV2, 27 instances (27/161) are misclassified in case of TFV3 and 35 instances (35/161) are misclassified in case of TFV4.

5.3.2.3. Experiment 3: To obtain classification performance of different TFVs (derived from Laws' masks of length 3, 5, 7 and 9) using SVM classifier.

In this experiment the classification performance of the feature set containing instances of TFV1, TFV2, TFV3 and TFV4 is evaluated using the SVM classifier. The results are shown in Table 5.12.

Table 5.12: Classification performance of different TFVs using SVM classifier for three-class breast tissue density classification

TFV(*l*)	**CM**				**OCA (%)**	**ICA_F (%)**	**ICA_{FG} (%)**	**ICA_{DG} (%)**
TFV1(30)		F	FG	DG	86.3	84.9	78.8	92.8
	F	46	5	2				
	FG	8	41	3				
	DG	0	4	52				
TFV2(75)	F	47	5	1	86.9	88.6	78.8	92.8
	FG	7	41	4				
	DG	0	4	52				
TFV3(30)	F	48	5	0	83.2	90.5	65.3	92.8
	FG	12	34	6				
	DG	0	4	52				
TFV4(75)	F	43	9	1	84.4	81.1	82.6	89.2
	FG	3	43	6				
	DG	0	6	50				

Note: TFV: Texture feature vector, *l*: Length of TFV, CM: Confusion Matrix, F: Fatty class, FG: Fatty-glandular class DG: Dense-glandular class, OCA: Overall classification accuracy; ICA_F: Individual class accuracy for fatty class. ICA_{FG}: Individual class accuracy for fatty-glandular class. ICA_{DG}: Individual class accuracy for dense-glandular class.

From the table it can be observed that a classification accuracy of 86.3 %, 86.9 %, 83.2 % and 84.4 % is achieved using TFV1, TFV2, TFV3 and TFV4, respectively. The individual class accuracy of fatty class is 84.9 %, 88.6 %, 90.5 % and 81.1 % for TFV1, TFV2, TFV3 and TFV4, respectively. For fatty-glandular class, the individual class accuracy is 78.8 %, 78.8 %, 65.3 % and 82.6 % for TFV1, TFV2, TFV3 and TFV4, respectively. For the dense-glandular class the individual class accuracy is 92.8 %, 92.8 %, 92.8 % and 89.2 % for TFV1, TFV2, TFV3 and TFV4, respectively.

Out of 161 instances of testing data, 22 instances (22/161) are misclassified in case of TFV1, 21 instances (21/161) are misclassified in case of TFV2, 27 instances (27/161) are misclassified in case of TFV3 and 25 instances (25/161) are misclassified in case of TFV4.

5.3.2.4. Experiment 4: To obtain the classification performance of different RTFVs (derived from Laws' masks of length 3, 5, 7 and 9) using PCA-kNN classifier.

In this experiment the classification performance of the feature set containing instances of RTFV1, RTFV2, RTFV3 and RTFV4 is evaluated using the PCA-kNN classifier. The results are shown in Table 5.13.

Table 5.13: Classification performance of different RTFVs using PCA-kNN classifier for three-class breast tissue density classification

RTFV (*l*)	**CM**				**OCA (%)**	**ICA_F (%)**	**ICA_{FG} (%)**	**ICA_{DG} (%)**
RTFV1(7)		F	FG	DG	85.0	83.0	82.6	83.9
	F	44	6	3				
	FG	4	43	5				
	DG	0	9	47				
RTFV2(7)	F	41	11	1	81.9	77.0	88.4	80.3
	FG	1	46	5				
	DG	1	10	45				
RTFV3(6)	F	44	5	4	86.9	83.0	86.5	91.0
	FG	1	45	6				
	DG	0	5	51				
RTFV4(10)	F	37	15	1	79.5	69.8	88.4	80.3
	FG	2	46	4				
	DG	2	9	45				

Note: RTFV: Reduced texture feature vector, *l*: Optimum number of PCs, CM: Confusion Matrix, F: Fatty class, FG: Fatty-glandular class DG: Dense-glandular class, OCA: Overall classification accuracy; ICA_F: Individual class accuracy for fatty class. ICA_{FG}: Individual class accuracy for fatty-glandular class. ICA_{DG}: Individual class accuracy for dense-glandular class.

From the table it can be observed that a classification accuracy of 85.0 %, 81.9 %, 86.9 % and 79.5 % is achieved using RTFV1, RTFV2, RTFV3 and RTFV4, respectively. The individual class accuracy of fatty class is 83.0 %, 77.0 %, 83.0 % and 69.8 % for RTFV1, RTFV2, RTFV3 and RTFV4, respectively. For fatty-glandular class, the individual class accuracy is 82.6 %, 88.4 %, 86.5 % and 88.4 % for RTFV1, RTFV2, RTFV3 and RTFV4, respectively. For the dense-glandular class the individual class accuracy is 83.9 %, 80.3 %, 91.0 % and 80.3 % for RTFV1, RTFV2, RTFV3 and RTFV4, respectively.

Out of 161 instances of testing data, 27 instances (27/161) are misclassified in case of RTFV1, 29 instances (29/161) are misclassified in case of RTFV2, 21 instances (21/161) are misclassified in case of RTFV3 and 33 instances (33/161) are misclassified in case of RTFV4.

5.3.2.5. Experiment 5: To obtain classification performance of different RTFVs (derived from Laws' masks of length 3, 5, 7 and 9) using PCA-PNN classifier.

In this experiment the classification performance of the feature set containing instances of RTFV1, RTFV2, RTFV3 and RTFV4 is evaluated using the PCA-PNN classifier. The results are shown in Table 5.14.

Table 5.14: Classification performance of different RTFVs using PCA-PNN classifier for three-class breast tissue density classification

RTFV (*l*)	**CM**				**OCA (%)**	**ICA_F (%)**	**ICA_{FG} (%)**	**ICA_{DG} (%)**
RTFV1(6)		F	FG	DG	83.8	84.9	90.3	76.7
	F	45	8	0				
	FG	4	47	1				
	DG	2	11	43				
RTFV2(9)	F	40	13	0	77.6	75.4	88.4	69.6
	FG	2	46	4				
	DG	7	10	39				
RTFV3(6)	F	46	7	0	85.0	86.7	90.3	78.5
	FG	3	47	2				
	DG	2	10	44				
RTFV4(10)	F	40	13	0	74.5	75.4	86.5	62.5
	FG	7	45	0				
	DG	11	10	35				

Note: RTFV: Reduced texture feature vector, *l*: Optimum number of PCs, CM: Confusion Matrix, F: Fatty class, FG: Fatty-glandular class DG: Dense-glandular class, OCA: Overall classification accuracy; ICA_F: Individual class accuracy for fatty class. ICA_{FG}: Individual class accuracy for fatty-glandular class. ICA_{DG}: Individual class accuracy for dense-glandular class.

From the table it can be observed that a classification accuracy of 83.8 %, 77.6 %, 85.0 % and 74.5 % is achieved using RTFV1, RTFV2, RTFV3 and RTFV4, respectively. The individual class accuracy of fatty class is 84.9 %, 75.4 %, 86.7 % and 75.4 % for RTFV1, RTFV2, RTFV3 and RTFV4, respectively. For fatty-glandular class, the individual class accuracy is 90.3 %, 88.4 %, 90.3 % and 86.5 % for RTFV1, RTFV2, RTFV3 and RTFV4, respectively. For the dense-glandular class the individual class accuracy is 76.7 %, 69.6 %, 78.5 % and 62.5 % for RTFV1, RTFV2, RTFV3 and RTFV4, respectively.

Out of 161 instances of testing data, 26 instances (26/161) are misclassified in case of RTFV1, 36 instances (36/161) are misclassified in case of RTFV2, 24 instances (24/161) are misclassified in case of RTFV3 and 41 instances (41/161) are misclassified in case of RTFV4.

5.3.2.6. Experiment 6: To obtain classification performance of different RTFVs (derived from Laws' masks of length 3, 5, 7 and 9) using PCA-SVM classifier.

In this experiment the classification performance of the feature set containing instances of RTFV1, RTFV2, RTFV3 and RTFV4 is evaluated using the PCA-SVM classifier. The results are shown in Table 5.15.

Table 5.15: Classification performance of different RTFVs using PCA-SVM classifier for three-class breast tissue density classification

RTFV (*l*)	**CM**				**OCA (%)**	**ICA_F (%)**	**ICA_{FG} (%)**	**ICA_{DG} (%)**
RTFV1(7)		F	FG	DG	87.5	84.9	84.6	92.8
	F	45	8	0				
	FG	5	44	3				
	DG	0	4	52				
RTFV2(9)	F	43	9	1	85.7	81.1	86.5	89.2
	FG	5	45	2				
	DG	1	5	50				
RTFV3(6)	F	46	7	0	86.3	86.7	78.8	92.8
	FG	6	41	5				
	DG	0	4	52				
RTFV4(10)	F	44	9	0	85.7	83.0	82.6	91.0
	FG	5	43	4				
	DG	0	5	51				

Note: RTFV: Reduced texture feature vector, *l*: Optimum number of PCs, CM: Confusion Matrix, F: Fatty class, FG: Fatty-glandular class DG: Dense-glandular class, OCA: Overall classification accuracy; ICA_F: Individual class accuracy for fatty class. ICA_{FG}: Individual class accuracy for fatty-glandular class. ICA_{DG}: Individual class accuracy for dense-glandular class.

From the table it can be observed that a classification accuracy of 87.5 %, 85.7 %, 86.3 % and 85.7 % is achieved using RTFV1, RTFV2, RTFV3 and RTFV4, respectively. The individual class accuracy of fatty class is 84.9 %, 81.1 %, 86.7 % and 83.0 % for RTFV1, RTFV2, RTFV3 and RTFV4, respectively. For fatty-glandular class, the individual class accuracy is 84.6 %, 86.5 %, 78.8 % and 82.6 % for RTFV1, RTFV2, RTFV3 and RTFV4, respectively. For the dense-glandular class the individual class accuracy is 92.8 %, 89.2 %, 92.8 % and 91.0 % for RTFV1, RTFV2, RTFV3 and RTFV4, respectively.

Out of 161 instances of testing data, 19 instances (19/161) are misclassified in case of RTFV1, 23 instances (23/161) are misclassified in case of RTFV2, 22 instances (22/161) are misclassified in case of RTFV3 and 23 instances (23/161) are misclassified in case of RTFV4.

5.4. Concluding Remarks

From the results obtained from the above experiments, it can be observed that for two-class breast tissue density, PCA-kNN classifier achieves highest classification accuracy of 95.6 % using first 8 PCs. Thus, it can be concluded that for two-class breast tissue density classification, first 8 PCs obtained by applying PCA to the TFV derived from Laws' mask of length 5 are sufficient to account for the textural changes exhibited by the fatty and dense breast tissue.

For three-class breast tissue density classification, it can be observed from the above experiments that the highest classification accuracy of 87.5 % is achieved using the PCA-SVM classifier and first 7 PCs derived from Laws' texture features using Laws' mask of length 3. Thus it can be said that for accounting the textural changes exhibited by different density patterns, first 7 PCs derived from Laws' mask of length 3 are sufficient.

Chapter 6

CAD System Design for Breast Tissue Density Classification Using Multiresolution Texture Features

6.1. Introduction

It has been well established that the risk of breast cancer development is associated with increased breast density. Therefore, characterization of breast tissue density is clinically significant. In the present work, texture features computed in transform domain over various scales have been used for efficient description of texture information in medical images, as scale is considered to be a dominant aspect of texture.

6.2. Proposed CAD System Design

The block diagram of the proposed CAD system design for two-class and three-class breast tissue density classification is shown in Figure 6.1.

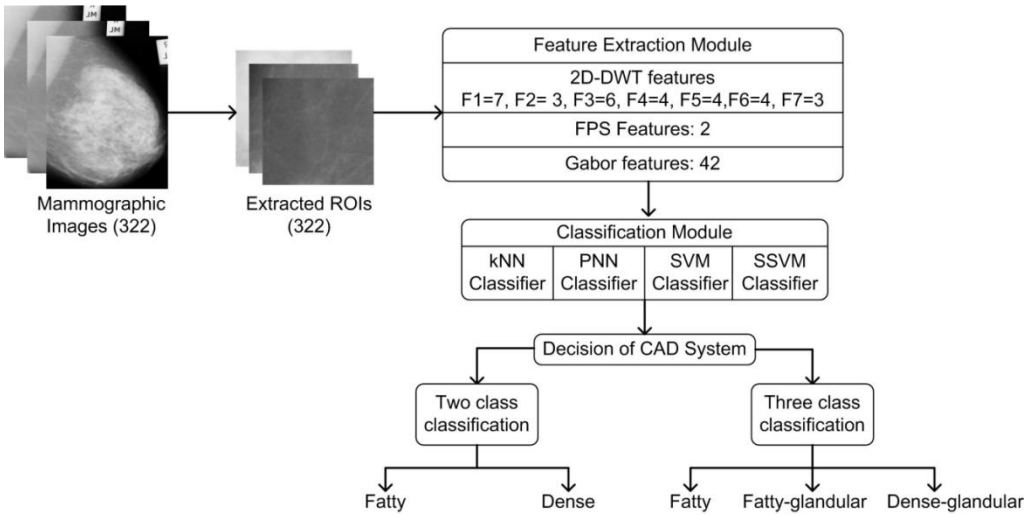

Figure 6.1 Proposed CAD system design using multiresolution texture features for two-class and three-class breast tissue density classification.

For the design of the proposed CAD system, multiresolution texture features like 2D DWT, FPS and GWT features have been extracted from each ROI image. The wavelet based texture features have been derived from ten different compact support wavelet filters like Haar (db1), Daubechies (db4 and db6), Coiflets (coif1 and coif2), Symlets (sym3 and sym 5) and Biorthogonal (bior3.1, bior3.3 and bior4.4). When 2D-DWT decomposition upto 2^{nd} level is applied to an ROI image, seven subimages (one approximate subimage and six orientation selective detail subimages) are generated.

From each subimage, normalized energy is calculated which is then used to form different TFVs. The TFVs derived are described in Table 6.1.

Table 6.1: Description of TFVs

TFV	Wavelet energy features	*l*
TFV1	$\left(\frac{\|A_2\|_F^2}{area(A_2)}, \frac{\left\|D_2^{(h)}\right\|_F^2}{area(D_2^{(h)})}, \frac{\left\|D_2^{(v)}\right\|_F^2}{area(D_2^{(v)})}, \frac{\left\|D_2^{(d)}\right\|_F^2}{area(D_2^{(d)})}, \frac{\left\|D_1^{(h)}\right\|_F^2}{area(D_1^{(h)})}, \frac{\left\|D_1^{(v)}\right\|_F^2}{area(D_1^{(v)})}, \frac{\left\|D_1^{(d)}\right\|_F^2}{area(D_1^{(d)})}\right)$	7
TFV2	$\left(\frac{\left\|D_1^{(h)}\right\|_F^2}{area(D_1^{(h)})}, \frac{\left\|D_1^{(v)}\right\|_F^2}{area(D_1^{(v)})}, \frac{\left\|D_1^{(d)}\right\|_F^2}{area(D_1^{(d)})}\right)$	3
TFV3	$\left(\frac{\left\|D_2^{(h)}\right\|_F^2}{area(D_2^{(h)})}, \frac{\left\|D_2^{(v)}\right\|_F^2}{area(D_2^{(v)})}, \frac{\left\|D_2^{(d)}\right\|_F^2}{area(D_2^{(d)})}, \frac{\left\|D_1^{(h)}\right\|_F^2}{area(D_1^{(h)})}, \frac{\left\|D_1^{(v)}\right\|_F^2}{area(D_1^{(v)})}, \frac{\left\|D_1^{(d)}\right\|_F^2}{area(D_1^{(d)})}\right)$	6
TFV4	$\left(\frac{\left\|D_1^{(h)}\right\|_F^2}{area(D_1^{(h)})}, \frac{\left\|D_1^{(v)}\right\|_F^2}{area(D_1^{(v)})}, \frac{\left\|D_1^{(d)}\right\|_F^2}{area(D_1^{(d)})}, \frac{\left\|D_2^{(d)}\right\|_F^2}{area(D_2^{(d)})}\right)$	4
TFV5	$\left(\frac{\|A_2\|_F^2}{area(A_2)}, \frac{\left\|D_1^{(h)}\right\|_F^2}{area(D_1^{(h)})}, \frac{\left\|D_1^{(v)}\right\|_F^2}{area(D_1^{(v)})}, \frac{\left\|D_1^{(d)}\right\|_F^2}{area(D_1^{(d)})}\right)$	4
TFV6	$\left(\frac{\|A_2\|_F^2}{area(A_2)}, \frac{\left\|D_2^{(h)}\right\|_F^2}{area(D_2^{(h)})}, \frac{\left\|D_2^{(v)}\right\|_F^2}{area(D_2^{(v)})}, \frac{\left\|D_2^{(d)}\right\|_F^2}{area(D_2^{(d)})}\right)$	4
TFV7	$\left(\frac{\left\|D_2^{(h)}\right\|_F^2}{area(D_2^{(h)})}, \frac{\left\|D_2^{(v)}\right\|_F^2}{area(D_2^{(v)})}, \frac{\left\|D_2^{(d)}\right\|_F^2}{area(D_2^{(d)})}\right)$	3
TFV8	Combined TFV consisting of best TFV out of TFV1-TFV7 based on classification results and FPS features	2+*l*
TFV9	TFV consisting of Gabor features	42

Note: TFVF: Texture feature vector *l*: Length of TFV, A: Approximate subimage, D: Detail subimage, h: Horizontal direction, v: Vertical direction, d: Diagonal direction, $\|.\|_F$: Frobenius norm. A_i or D_i: i is the level of decomposition.

Two features namely angular sum and radial sum are extracted from ROIs using FPS.

From the group of 21 wavelets formed using 2D-DWT, two texture features, mean and standard deviation are extracted from the 21 feature images.

These derived TFVs are then fed to classifiers like kNN, PNN, SVM and SSVM for two-class and three-class breast tissue density classification.

6.3. Experimental Workflow and Results

Rigorous experiments were carried out to evaluate the performance of proposed CAD system for two-class and three-class breast tissue density classification. A brief description of these experiments is given in Table 6.2 and 6.3, respectively.

Table 6.2: Description of experiments carried out for two-class breast tissue density classification

Experiment 1:	To obtain the classification performance of TFV1-TFV7 derived from various compact support wavelet filters for two-class breast tissue density classification using different classifiers
Experiment 2:	To obtain the classification performance of TFV8 for two-class breast tissue density classification using different classifiers
Experiment 3:	To obtain the classification performance of TFV9 for two-class breast tissue density classification using different classifiers

Note: TFV: Texture feature vector.

Table 6.3: Description of experiments carried out for three-class breast tissue density classification

Experiment 1:	To obtain the classification performance of TFV1-TFV7 derived from various compact support wavelet filters for three-class breast tissue density classification using different classifiers
Experiment 2:	To obtain the classification performance of TFV8 for three-class breast tissue density classification using different classifiers
Experiment 3:	To obtain the classification performance of TFV9 for three-class breast tissue density classification using different classifiers

Note: TFV: Texture feature vector.

6.3.1. Experiments carried out for two-class breast tissue density classification

6.3.1.1. Experiment 1: To obtain the classification performance of TFV1-TFV7 derived from various compact support wavelet filters for two-class breast tissue density classification using different classifiers.

In this experiment, the performance of various compact support wavelet filters has been evaluated using kNN, PNN, SVM and SSVM classifiers for two-class breast tissue density classification. The results are shown in Table 6.4.

Table 6.4: Classification performance of TFV1-TFV7 using kNN, PNN, SVM and SSVM classifiers for two-class breast tissue density classification

TFV (*l*)	Max. Acc. (%) (Classifier)	Wavelet Filter	Min. Acc. (%) (Classifier)	Wavelet Filter
TFV1 (7)	96.2 (kNN)	db1	83.8 (PNN)	db4, bior3.3
TFV2 (3)	88.8 (SSVM)	db1	66.4 (kNN, SVM)	db1, bior3.3
TFV3 (6)	91.3 (SSVM)	db1	73.2 (kNN)	db6
TFV4 (4)	87.5 (SSVM)	db1	68.3 (SVM)	bior3.1
TFV5 (4)	92.5 (SSVM)	db1	79.5 (PNN)	db4, sym3
TFV6 (4)	94.4 (kNN)	db1	83.8 (PNN)	db4, sym3, sym5
TFV7 (3)	89.4 (SSVM)	db1	70.1 (kNN)	coif1

Note: TFV: Texture feature vector *l*: Length of TFV, Max. Acc.: Maximum accuracy, Min. Acc.: Minimum accuracy.

It is observed that for all seven TFVs maximum classification accuracy is obtained using the db1 (Haar) wavelet filter. It can also be seen that the highest accuracy of 96.2 % is achieved with TFV1 using kNN classifier. The minimum

accuracy of 66.4 % is achieved for db1 and bior3.3 wavelet filters using the kNN and SVM classifiers, respectively.

6.3.1.2. Experiment 2: To obtain the classification performance of TFV8 for two-class breast tissue density classification using different classifiers.

In this experiment, the performance of TFV8 i.e. combined TFV consisting of wavelet based texture features yielding maximum accuracy in Experiment 1 and FPS features has been evaluated using different classifiers. The results are shown in Table 6.5. It can be observed from the table that for TFV8, the overall classification accuracy values of 80.7 %, 85.0 %, 86.3 % and 90.0 % are achieved using kNN, PNN, SVM and SSVM classifiers, respectively. It can also be observed that the highest in individual class accuracy for fatty class is 77.3 % with SSVM classifier and highest individual class accuracy for dense class is 96.2 %, using SSVM classifier.

Out of total 161 testing instances, 31 instances (31/161) are misclassified in case of kNN, 24 instances (24/161) are misclassified in case of PNN, 22 instances (16/161) are misclassified in case of SVM and 16 instances (16/161) are misclassified in case of SSVM classifier.

Table 6.5: Classification performance of TFV8 using kNN, PNN, SVM and SSVM classifiers for two-class breast tissue density classification

Classifier	**CM**			**OCA (%)**	**ICA_F (%)**	**ICA_D (%)**
kNN		F	D	80.7	66.0	87.9
	F	35	18			
	D	13	95			
PNN	F	34	19	85.0	64.1	95.3
	D	5	103			
SVM	F	38	15	86.3	71.6	93.5
	D	7	101			
SSVM	F	41	12	90.0	77.3	96.2
	D	4	104			

Note: CM: Confusion matrix, F: Fatty class, D: Dense class, OCA: Overall classification accuracy; ICA_F: Individual class accuracy for fatty class. ICA_D: Individual class accuracy for dense class.

6.3.1.3. Experiment 3: To obtain the classification performance of TFV9 for two-class breast tissue density classification using different classifiers.

In this experiment, the performance of texture feature vector derived from Gabor based features has been evaluated using different classifiers. The results are shown in Table 6.6.

Table 6.6: Classification performance of TFV9 using kNN, PNN, SVM and SSVM classifiers for two-class breast tissue density classification

Classifier	CM			OCA (%)	ICA_F (%)	ICA_D (%)
kNN		F	D	90.6	83.0	94.4
	F	44	9			
	D	6	102			
PNN	F	43	10	86.9	81.1	89.8
	D	11	97			
SVM	F	43	10	90.6	81.1	95.3
	D	5	103			
SSVM	F	45	8	92.5	84.9	96.2
	D	4	104			

Note: CM: Confusion matrix, F: Fatty class, D: Dense class, OCA: Overall classification accuracy; ICA_F: Individual class accuracy for fatty class. ICA_D: Individual class accuracy for dense class.

It can be observed from the table that for Gabor based texture features, the overall classification accuracy values of 90.6 %, 86.9 %, 90.6 % and 92.5 % are achieved using kNN, PNN, SVM and SSVM classifiers, respectively. It can also be observed that the highest individual class accuracy for fatty class is 84.9 % with SSVM classifier and highest individual class accuracy for dense class is 96.2 %, using SSVM classifier. Out of total 161 testing instances, 15 instances (15/161) are misclassified in case of kNN, 21 instances (21/161) are misclassified in case of PNN, 15 instances (15161) are misclassified in case of SSVM classifier.

6.3.2. Experiments carried out for three-class breast tissue density classification

6.3.2.1. Experiment 1: To obtain the classification performance of TFV1-TFV7 derived from various compact support wavelet filters for three-class breast tissue density classification using different classifiers.

In this experiment, the performance of various compact support wavelet filters has been evaluated using kNN, PNN, SVM and SSVM classifiers for three-class breast tissue density classification. The results are shown in Table 6.7.

Table 6.7: Classification performance of TFV1-TFV7 using kNN, PNN, SVM and SSVM classifiers for three-class breast tissue density classification

TFV (*l*)	Max. Acc. (%) (Classifier)	Wavelet Filter	Min. Acc. (%) (Classifier)	Wavelet Filter
TFV1 (7)	88.8 (kNN)	db1	76.3 (SVM)	db4
TFV2 (3)	80.7 (SSVM)	db1	55.9 (kNN)	db1
TFV3 (6)	83.2 (SVM)	db1	60.8 (kNN)	db6
TFV4 (4)	76.4 (SSVM)	db1	57.7 (kNN)	bior3.3
TFV5 (4)	85.7 (PNN)	db1	73.2 (kNN)	db4, bior3.3
TFV6 (4)	89.4 (SSVM)	db1	63.3 (SSVM)	bior3.3
TFV7 (3)	81.9 (SSVM)	db1	56.5 (kNN)	coif1

Note: TFV: Texture feature vector *l*: Length of TFV, Max. Acc.: Maximum accuracy, Min. Acc.: Minimum accuracy.

It is observed that for all seven TFVs maximum classification accuracy is obtained using the db1 (Haar) wavelet filter. It can also be seen that the highest accuracy of 89.4 % is achieved with TFV6 using SSVM classifier. The minimum accuracy of 55.9 % is achieved for db1 wavelet filter using the kNN classifier.

6.3.2.2. Experiment 2: To obtain the classification performance of TFV8 for three-class breast tissue density classification using different classifiers.

In this experiment, the performance of TFV8 i.e. combined TFV consisting of wavelet based texture features yielding maximum accuracy in Experiment 1 and FPS features have been evaluated using different classifiers. The results are shown in Table 6.8.

Table 6.8: Classification performance of TFV8 using kNN, PNN, SVM and SSVM classifiers for three-class breast tissue density classification

Classifier	**CM**				**OCA (%)**	**ICA_F (%)**	**ICA_{FG} (%)**	**ICA_{DG} (%)**
kNN		F	FG	DG	90.0	94.3	78.8	96.4
	F	50	3	0				
	FG	6	41	5				
	DG	0	2	54				
PNN	F	47	5	1	84.4	88.6	80.7	87.5
	FG	8	42	2				
	DG	0	9	49				
SVM	F	43	7	3	78.8	81.1	61.5	92.8
	FG	11	32	9				
	DG	0	5	52				
SSVM	F	46	6	1	88.2	86.7	90.3	89.2
	FG	2	47	3				
	DG	0	6	50				

Note: CM: Confusion matrix, F: Fatty class, FG: Fatty–glandular class, DG: Dense-glandular class, OCA: Overall classification accuracy; ICA_F: Individual class accuracy for fatty class, $ICA_{FG:}$ Individual class accuracy for fatty-glandular class, ICA_{DG}: Individual class accuracy for dense-glandular class.

It can be observed from the table that for TFV8, the overall classification accuracy values of 90.0 %, 84.4 %, 78.8 % and 88.2 % are achieved using kNN, PNN, SVM and SSVM classifiers, respectively. It can also be observed that the highest in individual class accuracy for fatty class is 94.3 % with kNN classifier, for the fatty-glandular class, the highest individual class accuracy is 90.3 % and the highest individual class accuracy for dense class is 96.4 %, using kNN classifier. Out of total 161 testing instances, 16 instances (16/161) are misclassified in case of kNN, 25 instances (25/161) are misclassified in case of PNN, 34 instances (34/161) are misclassified in case of SVM and 18 instances (18/161) are misclassified in case of SSVM classifier.

6.3.2.3. Experiment 3: To obtain the classification performance of TFV9 for three-class breast tissue density classification using different classifiers.

In this experiment, the performance of texture feature vector derived from Gabor based features has been evaluated using different classifiers. The results are shown in Table 6.9.

Table 6.9: Classification performance of TFV9 using kNN, PNN, SVM and SSVM classifiers for three-class breast tissue density classification

Classifier	CM				OCA (%)	ICA_F (%)	ICA_{FG} (%)	ICA_{DG} (%)
kNN		F	FG	DG	86.9	83.0	78.8	98.2
	F	44	6	3				
	FG	4	41	7				
	DG	0	1	55				
PNN	F	41	10	2	84.4	77.3	80.7	94.6
	FG	2	42	8				
	DG	0	3	53				
SVM	F	37	15	1	81.3	69.8	82.6	96.2
	FG	1	43	8				
	DG	1	4	51				
SSVM	F	49	3	1	83.8	92.4	65.3	92.8
	FG	7	34	11				
	DG	2	2	52				

Note: CM: Confusion matrix, F: Fatty class, FG: Fatty–glandular class, DG: Dense-glandular class, OCA: Overall classification accuracy; ICA_F: Individual class accuracy for fatty class, $ICA_{FG:}$ Individual class accuracy for fatty-glandular class, ICA_{DG}: Individual class accuracy for dense-glandular class.

It can be observed from the table that for Gabor based texture features, the overall classification accuracy of 86.9 %, 84.4 %, 81.3 % and 83.8 % is achieved using kNN, PNN, SVM and SSVM classifiers, respectively. It can also be observed that the highest individual class accuracy for fatty class is 92.4 % with SSVM classifier, for the fatty-glandular class, the highest individual class accuracy achieved is 82.6 % with SVM classifier and highest individual class accuracy for dense class is 98.2 %, using kNN classifier. Out of total 161 testing instances, 21 instances (21/161) are misclassified in case of kNN, 25 instances (25/161) are misclassified in case of PNN, 30 instances (30/161) are misclassified in case of SVM and 26 instances (26/161) are misclassified in case of SSVM classifier.

6.4. Concluding Remarks

From the results obtained from the above experiments, it can be observed that for two-class breast tissue density, kNN based CAD system design employing wavelet based texture features is the best choice for discriminating between different density

patterns exhibited by the breast tissue. The texture features are computed TFV1 derived from Haar wavelet filter.

For three-class breast tissue density classification, it can be observed from the above experiments that highest classification accuracy of 90.0 % is achieved using the kNN classifier with TFV8, derived by combining TFV6 (obtained from db1 (Haar) wavelet filter) and FPS features. Thus a total of 9 features are sufficient to discriminate between the different breast tissue density patterns.

Chapter 7

Conclusion and Future Scope

The present work has been carried out for two-class and three-class breast tissue density classification of digitized mammograms taken from the MIAS database keeping in mind the fact that increased breast density is strongly correlated with the risk of breast cancer development. Accordingly, different CAD system designs have been proposed in the present work for two-class and three-class breast tissue density classification to provide radiologists with a second opinion tool.

7.1. Conclusion- Design of an Efficient CAD System for Two-Class Breast Tissue Density Classification

For designing an efficient CAD system for two-class breast tissue density classification, various CAD system designs based on statistical features, Laws' TEMs and multiresolution texture features have been proposed in the present work. The performance of these CAD system designs has been compared in Table 7.1

Table 7.1: Performance comparison of CAD system designs for two-class breast tissue density classification

TFV	Classifier	CAD design	OCA (%)
Statistical features	PCA-SSVM	CAD system design based on statistical features	94.4
RTFV2	PCA-kNN	CAD system design based on texture features derived from Laws' masks	95.6
TFV1 (db1)	kNN	CAD system design based on multiresolution texture features	96.2

Note: TFV: Texture feature vector, RTFV: Reduced texture feature vector, OCA: Overall classification accuracy.

From the above table it can be observed that CAD system design based on wavelet based multiresolution texture features computed from db1 wavelet filter achieves maximum classification of 96.2 % out of all the proposed CAD system designs for two-class breast tissue density. It can that be concluded that the wavelet based texture features are thus most efficient texture features to account for the textural changes exhibited by fatty and dense breast tissue when fed to kNN classifier for predicting the labels unknown testing instances of the mammographic images.

7.2. Conclusion-Design of an Efficient CAD System for Three-Class Breast Tissue Density Classification

For the design of an efficient CAD system for three-class breast tissue density classification, exhaustive experimentation was carried out in the present work by using statistical features, Laws' TEMs and multiresolution texture features. The performance of the proposed CAD system designs based on these features is compared in Table 7.2.

Table 7.2: Performance comparison of CAD system designs for three-class breast tissue density classification

TFV	Classifier	CAD design	OCA (%)
Statistical features	PCA-SVM	CAD system design based on statistical features	86.3
RTFV1	PCA-SVM	CAD system design based on texture features derived from Laws' masks	87.5
TFV8 (TFV6 (db1)+FPS)	kNN	CAD system design based on multiresolution texture features	90.0

Note: TFV: Texture feature vector, RTFV: Reduced texture feature vector, OCA: Overall classification accuracy.

From the above table it can be observed that CAD system design based on combined TFV derived from wavelet based multiresolution texture features computed from db1 wavelet filter and FPS features achieves maximum classification of 90.0 % with kNN classifier out of all the proposed CAD system designs for three-class breast tissue density. It can be concluded that the multiresolution texture features when combined together give improved classification accuracy than the individual TFVs and efficiently discriminate between the different breast tissue density patterns exhibited on the mammograms.

From the above discussion it can be concluded that multiresolution texture features efficiently classify the mammograms as per different breast tissue density patterns both for two-class classification problem as well as three-class classification problem achieving best results in comparison to CAD system designs based on other feature extraction models.

7.3. Limitations and Future Scope

The limitation of the present work is that it has been carried out on the MIAS database that consists of digitized mammographic images and not real data.

Following are the recommendations for future work:

(*i*) Till date the available image databases for analysis of mammographic density patterns consist of digitized images of the mammograms. Recently, a database, INbreast consisting of DICOM images [81] has been available and can be used to evaluate the performance of the proposed algorithms of density classification.

(*ii*) The present work has been carried out on images developed using X-rays as the imaging modality however, images acquired from MRI can also be used in the future to test the proposed algorithms.

(*iii*) In the present work, ROIs from the mammograms are extracted manually. An algorithm for automatic ROI extraction can be developed by employing various pattern recognition concepts to identify the center of the breast tissue and then extract an ROI of some specified size automatically.

(*iv*) The performance of the proposed algorithms remains to be tested on images of different resolutions.

Publications from the Present Work

Referred Journal Publications

1) Kriti and Jitendra Virmani, "Breast Density Classification Using Laws' Mask Texture Features", *International Journal of Biomedical Engineering and Technology*. (Publisher: Inderscience) [Minor revisions submitted].
2) Kriti and Jitendra Virmani, "Three Class Breast Tissue Density Classification of Mammograms using Multiresolution Texture Features", *CSI Transactions on ICT*. (Publisher: Springer) [Under Review].
3) Kriti and Jitendra Virmani, "Comparison of CAD Systems for Two-Class and Three-Class Breast Tissue Density Classification using Gabor Features", *Sadhana*. (Publisher: Springer) [Communicated].

Referred Conference Publications

1) Kriti and Jitendra Virmani, "Breast Tissue Density Classification using Wavelet Based Texture Descriptors", in *2nd International Conference on Computer and Communication Technologies*. [Accepted for Publication].

References

[1] K. Ganesan, U.R. Acharya, C.K. Chua, L.C. Min, T.K. Abraham and K.H. Ng, "Computer-aided breast cancer detection using mammograms: a review", *IEEE Reviews in Biomedical Engineering*, vol. 6, pp.77-98, 2013.

[2] What is cancer? *MNT Knowledge Center*, [online], http://www.medicalnewstoday.com/info/cancer-oncology/ (Accessed: 6 December 2014).

[3] Breast cancer awareness month in October, *World Health Organisation*, [online] 2012, http://www.who.int/cancer/events/breast_cancer_month/en/ (Accessed: 6 December 2014).

[4] Cancer stats: key stats, *Cancer Research UK*, [online], http://www.cancerresearchuk.org/cancer-info/cancerstats/keyfacts/ (Accessed: 8 December 2014).

[5] Globocan 2012: Estimated cancer incidence, mortality and prevalence worldwide, *International Agency for Research on Cancer*, [online], 2012, http://globocan.iarc.fr/Default.aspx (Accessed: 6 December 2014).

[6] J.N. Wolfe, "Breast patterns as an index of risk for developing breast cancer", *American Journal of Roentgenology*, vol. 126, pp.1130-1137, 1976.

[7] J.N. Wolfe. "Risk for breast cancer development determined by mammographic parenchymal pattern", *Cancer*, vol. 37, pp. 2486-2492, 1976

[8] N.F. Boyd and L.J. Martin, "Potential mechanism of breast cancer risk associated with mammographic density: hypothesis based on epidemiological evidence", *Breast Cancer Research*, vol. 10, pp. 201-214, 2008.

[9] N.F. Boyd, J.M. Rommens, K. Vogt, V. Lee, J.L. Hopper, M.J. Yaffe, and A.D. Paterson, "Mammographic breast density as an intermediate phenotype for breast cancer", *Lancet Oncology*, vol. 6, pp. 798-808, 2005.

[10] D.S. AlMousa, P.C. Brennan, E.A. Ryan, W.B. Lee, J. Tan and C. Mello-Thomas, "How mammographic breast density affects radiologists' visual search patterns", *Academic Radiology*, vol. 2, pp. 1386-1393, 2014.

[11] C. Colin, V. Prince and P.J. Valette, "Can mammographic assessments lead to consider density as a risk factor for breast cancer?" *European Journal of Radiology*, vol. 82, pp. 404-411, 2013.

[12] N.F. Boyd, L.J. Martin, S. Chavez, A. Gunasekara, A. Salleh, O. Melnichouk, M. Yaffe, C. Friedenreich, S. Minkin and M. Bronskill, "Breast tissue composition and

other risk factors for breast cancer in young women: a cross sectional study", *Lancet* Oncology, vol. 10, pp. 569-580, 2009.

[13] C.M. Vachon, C.H. vanGills, T.A. Sellers, K. Ghosh, S. Pruthi, K.R. Brandt and V.S. Pankratz, "Mammographic density, breast cancer risk and risk prediction", *Breast Cancer Research*, vol. 9, pp. 217-225, 2007.

[14] N.F. Boyd, G.A. Lockwood, J.W. Byng, D.L. Tritchler and M.J. Yaffe, "Mammographic densities and breast cancer risk", *Cancer Epidemiology, Biomarkers and Prevention*, vol. 7, pp.1133-1144, 1998.

[15] A. Eng, Z. Gallant, J. Shepherd, V. McCormack, J. Li, M. Dowsett, S. Vinnicombe, S. Allen and I. Silva, "Digital mammographic density and breast cancer risk: a case–control study of six alternative density assessment methods", *Breast Cancer Research*, vol. 16, pp. 439-452, 2014.

[16] C. Zhou, H.P. Chan, N. Petrick, M.A. Helvie, M.M. Goodsitt, B. Sahiner and L.M. Hadjiiski, "Computerized image analysis: Estimation of breast density on mammograms", *Medical Physics*, vol. 28, pp. 1056-1069, 2001.

[17] J.J. Heine, M.J. Carton and C.G. Scott, "An automated approach for estimation of breast density", *Cancer Epidemiology, Biomarkers and Prevention*, vol. 17, pp. 3090-3097, 2008.

[18] Understanding your mammogram report-BI-RADS categories, *American Cancer Society*, [online], http://www.cancer.org/healthy/findcancerearly/examandtestdescriptions/mammogramsandotherbreastimagingprocedures/mammograms-and-other-breast-imaging-procedures-mammo-report (Accessed: 15 December 2014).

[19] M.L. Giger, K. Doi, H. MacMahon, R.M. Nishikawa, K.R. Hoffman, C.J. Vyborny, R.A. Schmidt, H. Jia, K. Abe and X. Chen, "An intelligent workstation for computer-aided diagnosis, *Radiographics*, vol. 13, pp. 647-656, 1993.

[20] K. Doi, H. MacMahon, S. Katsuragawa, R.M. Nishikawa and Y. Jiang, "Computer-aided diagnosis in radiology: potential and pitfalls", *European Journal of Radiology*, vol. 31, pp. 97-109, 1997.

[21] G.D. Tourassi, "Journey toward computer-aided diagnosis: role of image texture analysis", *Radiology*, vol. 213, pp. 317-320, 1999.

[22] H.P. Chan, K. Doi, C.J. Vybrony, R.A. Schmidt, C. Metz, K.L. Lam, T. Ogura, Y. Wu and H. MacMahon, "Improvement in radiologists' detection of clustered micro-calcifications on mammograms: the potential of computer-aided diagnosis", *Instigative Radiology*, vol. 25, pp. 1102-1110, 1990.

[23] P. Miller and A. Astley, "Classification of breast tissue by texture analysis", *Image and Vision Computing*, vol. 10, pp. 277-282, 1992.

[24] K. Bovis and S. Singh, "Classification of mammographic breast density using a combined classifier paradigm", *4th International Workshop on Digital Mammography*, pp. 1-4, 2002.

[25] C. Castella, K. Kinkel, M.P. Eckstein, P.E. Sottas, F.R. Verdun and F.O. Bochud, "Semiautomatic mammographic parenchymal patterns classification using multiple statistical features", *Academic Radiology*, vol. 14, pp. 1486-1499, 2007.

[26] A. Oliver, J. Freixenet, R. Marti, J. Pont, E. Perez, E.R.E. Denton and R. Zwiggelaar, "A novel breast tissue density classification methodology". *IEEE Transactions on Information Technology in Biomedicine*, vol. 12, pp. 55-65, 2008.

[27] M. Mustra, M. Grgic, and K. Delac, "Breast density classification using multiple feature selection", *Auotomatika*, vol. 53, pp. 362-372, 2012.

[28] V. Sharma and S. Singh, "CFS–SMO based classification of breast density using multiple texture models", *Medical and Biological Engineering and Computing*, vol. 52, pp. 521-529, 2014.

[29] V. Sharma and S. Singh, "Automated classification of fatty and dense mammograms', *Journal of Medical Imaging and Health Informatics*, vol. 5, pp. 520-526 (7), 2015.

[30] L. Blot and R. Zwiggelaar, "Background texture extraction for the classification of mammographic parenchymal patterns", in *Proceedings of Conference on Medical Image Understanding and Analysis*, 2001, pp. 145-148.

[31] A. Bosch, X. Munoz, A. Oliver and J. Marti, "Modelling and classifying breast tissue density in mammograms", In *Computer Vision and Pattern Recognition, IEEE Computer Society Conference*, New York, USA, 2006, vol. 2, pp. 1552-1558.

[32] I. Muhimmah and R. Zwiggelaar, "Mammographic density classification using multiresolution histogram information", in *Proceedings of 5th International IEEE Special Topic Conference on Information Technology in Biomedicine* (ITAB), Ioannina, Greece, 2006, pp. 1-6.

[33] T.S. Subashini, V. Ramalingam and S. Palanivel, "Automated assessment of breast tissue density in digital mammograms", *Computer Vision and Image Understanding*, vol. 114, pp. 33-43, 2010.

[34] S.D. Tzikopoulos, M.E. Mavroforakis, H.V. Georgiou, N. Dimitropoulos and S. Theodoridis, "A fully automated scheme for mammographic segmentation and

classification based on breast density and asymmetry", *Computer Methods and Programs in Biomedicine*, vol. 102, pp. 47-63, 2010.

[35] J.B. Li, "Mammographic image based breast tissue classification with kernel self-optimized fisher discriminant for breast cancer diagnosis", *Journal of Medical Systems*, vol. 36, pp. 2235-2244, 2012.

[36] W.R. Silva and D. Menotti, "Classification of mammograms by the breast composition", in *Proceedings of the 2012 International Conference on Image Processing, Computer Vision, and Pattern Recognition (IPCV'12)*, 2012, pp. 1-6.

[37] N. Karssemeijer, "Automated classification of parenchymal patterns in mammograms", *Physics in Medicine and Biology*, vol. 43, pp. 365-378, 1998.

[38] X.H. Wang, W.F. Good, B.E. Chapman, Y.H. Chang, W.R. Poller, T.S. Chang and L.A. Hardesty, "Automated assessment of the composition of breast tissue revealed on tissue thickness corrected mammography", *American Journal of Roentgenology*, vol. 180, pp. 257-262, 2003.

[39] S. Petroudi, T. Kadir and M. Brady, "Automatic classification of mammographic parenchymal patterns: a statistical approach", in *Proceedings of 25th Annual International Conference of IEEE on Engineering in Medicine and Biology Society*, Cancun, Mexico, 2003, vol. 1, pp. 798-801.

[40] A. Oliver, J. Freixenet, A. Bosch, D. Raba and R. Zwiggelaar, "Automatic classification of breast tissue", in *Pattern Recognition and Image Analysis*, J.S. Maeques, et al., Eds., Berlin, Heidelberg: Springer, 2005, vol. 3523, pp. 431-438.

[41] H. Li, M.L. Giger, Z. Huo, O.I. Olopade, L. Lan, B.L. Weber and I. Bonta, "Computerized analysis of mammographic parenchymal patterns for assessing breast cancer risk: Effect of ROI size and location", *Medical Physics*, vol. 31, pp. 549-555, 2004.

[42] J. Suckling, J. Parker, D.R. Dance, S. Astley, I. Hutt, C.R.M. Boggis, I. Ricketts, E. Stamatakis, N. Cerneaz, S.L. Kok, P. Taylor, D. Betal and J. Savage, "The mammographic image analysis society digital mammogram database", in *Digital Mammography*, E.G. Gale et al., Eds., Berlin, Heidelberg: Springer, 1994, vol.1069, pp. 375-378.

[43] J. Virmani, V. Kumar, N. Kalra and N. Khandelwal, "A rapid approach for prediction of liver cirrhosis based on first order statistics", in *Proceedings of the IEEE International Conference on Multimedia, Signal Processing and Communication Technologies, IMPACT-2011*, Aligarh, India, 2011, pp. 212-215.

[44] J. Virmani, V. Kumar, N. Kalra and N. Khandelwal, "Prediction of cirrhosis based on singular value decomposition of gray level co-occurrence matrix and a neural network classifier", in *Proceedings of Development in E-systems Engineering, DeSE*, Dubai, 2011, pp. 146-151.

[45] M. Vasantha, V. Subbiah Bharathi and R. Dhamodharan, "Medical image feature extraction, selection and classification", *International Journal of Engineering Science and Technology*, vol. 2, pp. 2071-2076, 2010.

[46] P. Mohanaiah, P. Sathyanarayanam and L. Gurukumar, "Image texture feature extraction using GLCM approach", *International Journal of Scientific and Research Publications*, vol. 3, pp. 1-5, 2013.

[47] D.H. Xu, A.S. Kurani, J.D. Furst and D.S. Raicu, "Run-length encoding for volumetric texture", *Heart*, vol. 27, pp. 25-30, 2004.

[48] F. Albregtsen, "Statistical texture measures computed from gray level run length matrices", *Image*, vol.1, pp. 3-8, 1995.

[49] G. Castellano, L.Bonilha, L.M. Li and F. Cendes, "Texture analysis of medical images", *Clinical Radiology*, vol.59, pp. 1061-1069, 2004.

[50] M. Amadasun and R. King, "Textural features corresponding to textural properties", *IEEE Transactions on Systems, Man and Cybernetics*, vol. 19, pp. 1264-1274, 1989.

[51] J.S. Weszka, C.R. Dyer and A. Rosenfeld, "A comparative study of texture measures for terrain classification", *IEEE Transactions on Systems, Man and Cybernetics*, vol. 6, pp. 269-285, 1976.

[52] J.K. Kim and H.W. Park, "Statistical textural features for detection of microcalcifications in digitized mammograms", *IEEE Transactions on Medical Imaging*, vol. 18, 1999.

[53] K.I. Laws, "Rapid texture identification", in *Proceedings of SPIE Image Processing for Missile Guidance*, 1980, pp. 376-380.

[54] M. Rachidi, A. Marchadier, C. Gadois, E. Lespessailles, C. Chappard and C. L. Benhamou, "Laws' masks descriptors applied to bone texture analysis: an innovative and discriminant tool in osteoporosis", *Skeletal Radiology*, vol. 37, pp. 541-548, 2008.

[55] J. Virmani, V. Kumar, N. Kalra and N. Khandelwal, "Characterization of primary and secondary malignant liver lesions from B-mode ultrasound", *Journal of Digital Imaging*, vol. 26, pp. 1058-1070, 2008.

[56] J. Virmani, V. Kumar, N. Kalra and N. Khandelwal, "Prediction of cirrhosis from liver ultrasound B-mode images based on Laws' mask analysis", in *Proceedings of IEEE International Conference on Image Information Processing, ICIIP-2011*. Himachal Pradesh, India, 2011, pp. 1-5.

[57] J. Virmani, V. Kumar, N. Kalra and N. Khandelwal, "Neural network ensemble based CAD system for focal liver lesions from B-mode ultrasound", *Journal of Digital Imaging*, vol. 27, pp. 520-537, 2014.

[58] G.H. Seng, H.Y. Chai and T.T. Swee, "Research on Laws' mask texture analysis system reliability", *Reasearch Journal of Applied Sciences, Engineering and Technology*, vol. 7, pp. 4002-4007, 2014.

[59] J.G. Daugman, "An information-theoretic view of analog representations in the striate cortex", in *Computational* Neuroscience, E.L. Schwartz, Ed. Cambridge: MIT Press, 1990, pp.403-424.

[60] H. Yoshida, D.D. Casalino, B. Keserci, A. Coskun, O. Ozturk and A. Savranlar, "Wavelet packet based texture analysis for differentiating between benign and malignant liver tumors in ultrasound images", *Physics in Medicine and Biology*, vol. 48, pp. 3735-3753, 2003.

[61] X. Li, Z. Tian, "Wavelet energy signature: comparison and analysis", in *Neural Information Processing*, I. King, J. Wang, L.W. Chan and D.L. Wang, Eds., Heidelberg, Berlin: Springer, 2006, vol. 4233, pp. 474-480.

[62] J. Virmani, V. Kumar, N. Kalra and N. Khandelwal N, "SVM-based characterization of liver ultrasound images using wavelet packet texture descriptors", *Journal of Digital Imaging*, vol. 26, pp. 530-543, 2012.

[63] J. Virmani, V. Kumar, N. Kalra and N. Khandelwal, "Prediction of liver cirrhosis based on multiresolution texture descriptors from B–mode ultrasound", *International Journal of Convergence Computing*, vol. 1, pp. 19-37, 2013.

[64] C.C. Lee, and S.H. Chen, "Gabor wavelets and SVM classifier for liver diseases classification from CT images", in *Proceedings of IEEE International Conference on Systems, Man and Cybernetics*, Taipei, Taiwan, 2006, pp. 548-552.

[65] S.R. Amendolia, G. Cossu, M.L. Ganadu, B. Galois, G.L. Masala and G.M. Mura, "A comparative study of k-nearest neighbor, support vector machine and multi-layer perceptron for thalassemia screening", *Chemometrics and Intelligent Laboratory Systems*, vol. 69, pp. 13-20, 2003.

[66] J. Virmani, V. Kumar, N. Kalra and N. Khandelwal, "PCA-SVM based CAD system for focal liver lesion using B-mode ultrasound images", *Defence Science Journal*, vol. 63, pp. 478-486, 2013.

[67] J. Virmani, V. Kumar, N. Kalra and N. Khandelwal, "A comparative study of computer-aided classification systems for focal hepatic lesions from B-mode ultrasound, *Journal of Medical Engineering and Technology*, vol. 37, pp. 292-306, 2013.

[68] A. Yazdani, T. Ebrahimi and U. Hoffmann, "Classification of EEG signals using dempster shafer theory and a *k*-nearest neighbor classifier", in *Proceedings of 4th International IEEE EMBS Conference on Neural Engineering*, Antalya, Turkey, 2009, pp. 327-330.

[69] Y. Wu, K. Ianakiev and V. Govindaraju, "Improved kNN classification", *Pattern Recognition*, vol. 35, pp. 2311-2318, 2002.

[70] M.L. Zhang and Z.H. Zhou, "A kNN based algorithm for multilabel classification", in *Proceedings of IEEE International Conference on Granular Computing*, Beijing, China, 2005, vol. 2, pp. 718-721.

[71] D.F. Specht, "Probabilistic neural networks", *Neural Networks*, vol.1, pp. 109-118, 1990.

[72] D.F. Specht and H. Romsdahl, "Experience with adaptive probabilistic neural network and adaptive general regression neural network", in *Proceedings of the IEEE International Conference on Neural* Networks, Orlando, Florida, 1994, vol. 2, pp. 1203-1208.

[73] V.L. Georgiou, N.G. Pavlidis, K.E. Parsopoulos and M.N. Vrahatis, "Optimizing the performance of probabilistic neural networks in a bioinformatics task", in *Proceedings of the EUNITE 2004 Conference*, 2004, pp. 34-40.

[74] C.C. Chang and C. J. Lin, "LIBSVM, A library of support vector machines".

[75] J. Virmani, V. Kumar, N. Kalra and N. Khandelwal, "SVM based characterization of liver cirrhosis by singular value decomposition of GLCM matrix", *International Journal of Artificial Intelligence and Soft Computing*, vol. 3, pp. 276-296, 2013.

[76] A.E. Hassanien, N.E. Bendary, M. Kudelka and V. Snasel, "Breast cancer detection and classification using support vector machines and pulse coupled neural network", in *Proceedings of 3rd International Conference on Intelligent*

Human Computer Interaction IHCI 2011, Prague, Czech Republic, 2011, pp. 269-279.

[77] A.T.Azar and S.A. El-Said, "Performance analysis of support vector machine classifiers in breast cancer mammography recognition", *Neural Computing and Applications*, vol. 24, pp. 1163-1177, 2014.

[78] S.W. Purnami, A. Embong, J.M. Zain and S.P. Rahayu, "A new smooth support vector machine and its applications in diabetes disease diagnosis", *Journal of Computer Science*, vol. 5, pp. 1003-1008, 2009.

[79] Y.J. Lee and O.L. Mangasarian, "SSVM: a smooth support vector machine for classification", *Computational Optimization and Applications*, vol. 20, pp. 5-22, 2001

[80] Y.J. Lee and O.L. Mangasarian, SSVM toolbox. [online], http://research.cs. wisc.edu/dmi/ svm/ssvm/. (Accessed 30 March 2015).

[81] I.C. Moreira, I. Amaral, I. Dominques, A. Cardoso, M.J. Cardoso and J.S. Cardoso, "INbreast: toward a full-field digital mammographic database", *Academic Radiology*, vol. 19, pp. 236-248, 2012.

Appendix-A

Texture Features Used in the Present Work

A.1. Statistical features

A.1.1. First Order Statistics

For the individual pixel values x_i, the computed features are given as:

$$\text{Mean} = \frac{1}{N}\sum_i x_i$$

$$\text{Standard Deviation} = \frac{1}{\sqrt{N-1}}\left(\sum_i (x_i - \bar{x})^2\right)^{1/2}$$

$$\text{Third Moment} = \frac{1}{N\sigma^3}\sum_i (x_i - \bar{x})^3$$

$$\text{Uniformity} = \sum_i p(i)^2$$

$$\text{Entropy} = -\sum_i p(x_i) log_2 p(x_i)$$

$$\text{Smoothness} = 1 - \frac{1}{1+\sigma^2}$$

A.1.2. GLCM Features

$$\text{Angular Second Moment} = \sum_{i,j} {P_{ij}}^2$$

$$\text{Contrast} = \sum_{i,j} P_{i,j}(i-j)^2$$

$$\text{Correlation} = \sum_{i,j} P_{i,j}\left[\frac{(i-\mu_i)(j-\mu_j)}{\sigma_i \sigma_j}\right]$$

$$\text{Variance} = \sum_{i,j} P_{i,j}(i-\mu_i)^2$$

$$\text{Inverse Difference moment} = \sum_{i,j} \frac{P_{i,j}}{1+(i-j)^2}$$

$$\text{Sum Average} = f_{12} = \sum_{i=2}^{2N_g} i p_{x+y}(i)$$

$$\text{Sum Entropy} = f_{14} = -\sum_{i=2}^{2N_g} p_{x+y}(i)\log\left(p_{x+y}(i)\right)$$

$$\text{Sum Variance} = f_{13} = \sum_{i=2}^{2N_g} (i - f_{14})^2 p_{x+y}(i)$$

$$\text{Entropy} = -\sum_{i,j} p_{i,j} log(p_{i,j})$$

$$\text{Difference Variance} = -\sum_{i=0}^{N_g-1} (i - f_6)^2\, p_{x-y}(i)$$

$$\text{Difference Entropy} = f_{16} = -\sum_{i=0}^{N_g-1} p_{x-y}(i)\log\left(p_{x-y}(i)\right)$$

$$\text{Information Measure of Correaltion1} = \frac{-\sum_{i,j} p_{i,j}\left(\left(\log(p_{i,j})\right) - \log\left(p_x(i)p_y(i)\right)\right)}{\max\left(HX, HY\right)}$$

$$\text{Information Measure of Correaltion2} = f_{18} = \sqrt{1 - e^{-2(a-b)}}$$

$f_6 = \sum_{i,j} |i - j| p_{ij}$

$a = -\sum_{i,j} p_x(i)p_y(i)\log\left(p_x(i)p_y(i)\right)$

$b = -\sum_{i,j} p_{i,j}\log\left(p_x(i)p_y(i)\right)$

A.1.3. GLRLM Features

$$\text{Short Run Emphasis} = \sum_{i=1}^{G}\sum_{j=1}^{R} \frac{p(i,j|\theta)}{j^2} \Big/ \sum_{i=1}^{G}\sum_{j=1}^{R} p(i,j|\theta)$$

$$\text{Long Run Emphasis} = \sum_{i=1}^{G}\sum_{j=1}^{R} j^2 p(i,j|\theta) \Big/ \sum_{i=1}^{G}\sum_{j=1}^{R} p(i,j|\theta)$$

$$\text{Low Gray level Run Emphasis} = \sum_{i=1}^{G}\sum_{j=1}^{R} \frac{p(i,j|\theta)}{i^2} \Big/ \sum_{i=1}^{G}\sum_{j=1}^{R} p(i,j|\theta)$$

$$\text{High Gray level Run Emphasis} = \sum_{i=1}^{G}\sum_{j=1}^{R} i^2 p(i,j|\theta) \Big/ \sum_{i=1}^{G}\sum_{j=1}^{R} p(i,j|\theta)$$

$$\text{Short Run Low Gray Level Emphasis} = \sum_{i=1}^{G}\sum_{j=1}^{R}\frac{p(i,j|\theta)}{i^2 * j^2}\Big/\sum_{i=1}^{G}\sum_{j=1}^{R}p(i,j|\theta)$$

$$\text{Short Run High Gray Level Emphasis} = \sum_{i=1}^{G}\sum_{j=1}^{R}\frac{p(i,j|\theta) * i^2}{j^2}\Big/\sum_{i=1}^{G}\sum_{j=1}^{R}p(i,j|\theta)$$

$$\text{Long Run Low Gray Level Emphasis} = \sum_{i=1}^{G}\sum_{j=1}^{R}\frac{p(i,j|\theta) * j^2}{i^2}\Big/\sum_{i=1}^{G}\sum_{j=1}^{R}p(i,j|\theta)$$

$$\text{Long Run High Gray Level Emphasis} = \sum_{i=1}^{G}\sum_{j=1}^{R}p(i,j|\theta) * i^2 * j^2\Big/\sum_{i=1}^{G}\sum_{j=1}^{R}p(i,j|\theta)$$

$$\text{Gray level Non Uniformity} = \sum_{i=1}^{G}\left(\sum_{j=1}^{R}p(i,j|\theta)\right)^2\Big/\sum_{i=1}^{G}\sum_{j=1}^{R}p(i,j|\theta)$$

$$\text{Run Length Non Uniformity} = \sum_{i=1}^{R}\left(\sum_{j=1}^{G}p(i,j|\theta)\right)^2\Big/\sum_{i=1}^{G}\sum_{j=1}^{R}p(i,j|\theta)$$

$$\text{Run Percentage} = \frac{1}{n}\sum_{i=1}^{G}\sum_{j=1}^{R}p(i,j|\theta)$$

A.1.4. NGTDM Features

$$\text{Coarseness} = \left[\varepsilon + \sum_{i=0}^{i_{max}} p_i s(i)\right]^{-1}$$

$$\text{Contrast} = \left[\frac{1}{N_g(N_g-1)}\sum_{i=0}^{i_{max}}\sum_{j=0}^{j_{max}}p_i p_l (i-j)^2\right].\left[\frac{1}{n^2}\sum_{i=0}^{i_{max}}s(i)\right]$$

$$\text{Complexity} = \sum_{i=0}^{i_{max}}\sum_{j=0}^{j_{max}}\frac{|i-j|\left[p_i s(i) + p_j s(j)\right]}{n^2(p+p_i)}$$

$$\text{Strength} = \frac{\sum_{i=0}^{i_{max}}\sum_{j=0}^{j_{max}}\left(p_i + p_j\right)(i-j)^2}{\varepsilon + \sum_{i=0}^{i_{max}} s(i)}$$

$$\text{Business} = \sum_{i=0}^{i_{max}} p_i\, s(i) \Big/ \sum_{i=0}^{i_{max}} \sum_{j=0}^{j_{max}} ip_i - jp_j$$

A.1.5. SFM Features

$$\text{Coarseness} = c \Big/ \sum_{i.j} DSS(i,j) \Big/ n$$

$$\text{Contrast} = \left[\sum_{i,j} CON(i,j)/4 \right]^{1/2}$$

$$\text{Periodicity} = \frac{\bar{M}_{dss} - M_{dss}(valley)}{\bar{M}_{dss}}$$

$$\text{Roughness} = \left(D_f^{(h)} + D_f^{(v)} \right)/2$$

$DSS(\delta) \equiv E\{[I(x,y) - I(x+\Delta x, y+\Delta y]\}$

$CON(\delta) \equiv E\{[I(x,y) - I(x+\Delta x, y+\Delta y)]^2\}$

$\bar{M}_{dss}$: Mean of all elements in M_{dss} and M_{dss} (valley): Deepest valley in the matrix

D_f: Fractal dimension in horizontal and vertical direction.

A.1.6. GLDS Features

$$Homogenity = \sum_{i,j} \frac{P_{i,j}}{1 + (i-j)^2}$$

$$Contrast = \sum_{i,j} P_{ij}(i-j)^2$$

$$Energy = \sqrt{\sum_{i.j} P_{ij}^2}$$

$$Entropy = -\sum_{i,j} p_{i,j} log(p_{i,j})$$

$$Mean = \frac{1}{m} \sum_{i} iP_{ij}$$

A.2. Signal Processing Methods based Features

A.2.1. Laws' Texture Features

Laws' masks of lengths 3, 5, 7 and 9 are used to compute different features. A description of these masks is given below.

Table 1: Description of Laws' masks of different lengths

Length of 1-D filter	1-D filter coefficients	No. of 2D Laws' masks	No. of TR images
3	L3=[1, 2, 1] E3=[-1, 0, 1] S3=[-1, 2, -1]	9	6
5	L5= [1, 4, 6, 4, 1] E5= [-1, -2, 0, 2, 1] S5= [-1, 0, 2, 0, -1] W5= [-1, 2, 0, -2 1] R5= [1, -4, 6, -4, 1]	25	15
7	L7= [1, 6, 15, 20, 15, 6, 1] E7= [-1 -4, -5, 0, 5, 4, 1] S7= [-1, -2, 1, 4, 1, -2, -1]	9	6
9	L9= [1, 8, 28, 56, 70, 56, 28, 8, 1] E9= [1, 4, 4, -4, -10, -4, 4, 4, 1] S9= [1, 0, -4, 0, 6, 0, -4, 0, 1] W9= [1, -4, 4, -4, -10, 4, 4, -4, 1] R9= [1, -8, 28, -56, 70, -56, 28, -8, 1]	25	15

Note: TR: rotation invariant texture images.

As an example Laws' mask of length 5 is used for explanation purposes. The ROIs are convolved with each of the above twenty five 2D Laws' masks.

For example an ROI of size M × N (200× 200) is convolved with the mask S5S5 to form texture image (TI_{S5S5}).

$$TI_{S5S5} = ROI \otimes S5S5$$

The mask L5L5 has zero mean and is used to form contrast invariant texture images (TIs).

$$Normalize(TI_{mask}) = \frac{TI_{mask}}{TI_{L5L5}}$$

The normalized TIs are passed through a 15 × 15 square window to derive 25 texture energy images (TEMs). The TEM filters perform moving average non-linear filtering operation, i.e.

$$TEM_{i,j} = \sum_{u=-7}^{7} \sum_{v=-7}^{7} \left| Normalize(TI_{i+u,j+v}) \right|$$

Out of 25 TEMs 15 rotationally invariant texture energy images (TRs) are obtained by averaging, i.e.

$$TR_{S5L5} = \frac{TEM_{S5L5} + TEM_{L5S5}}{2}$$

From the derived TRs five statistical parameters i.e. mean, standard deviation, skewness, kurtosis and entropy are computed, thus 75 Laws' texture features (15 TRs × 5 statistical parameters) are computed for each ROI. These statistical parameters are defined as:

$$Mean = \frac{\sum_{i=0}^{M}\sum_{j=0}^{N}(TR_{i,j})}{M \times N}$$

$$SD = \sqrt{\frac{\sum_{i=0}^{M}\sum_{j=0}^{N}(TR_{i,j} - Mean)^2}{M \times N}}$$

$$Skewness = \frac{\sum_{i=0}^{M}\sum_{j=0}^{N}(TR_{i,j} - Mean)^3}{M \times N \times SD^3}$$

$$Kurtosis = \frac{\sum_{i=0}^{M}\sum_{j=0}^{N}(TR_{i,j} - Mean)^4}{M \times N \times SD^4} - 3$$

$$Entropy = \frac{\sum_{i=0}^{M}\sum_{j=0}^{N}(TR_{i.j})^2}{M \times N}$$

A.3. Transform Domain based Features

A.3.1. Wavelet based Texture Features

Normalized energy calculated for each subimage.

For approximate subimage at i^{th} level of decomposition

$$Normalized\ Energy = \frac{\|A_i\|_F^2}{area\ (A_i)}$$

For detailed subimage in *k^{th} direction and at i^{th}* level of decomposition

$$Normalized\ Energy = \frac{\left\|D_i^{(k)}\right\|_F^2}{area\left(D_i^{(k)}\right)}$$

A.3.2. FPS Features

$$RadialSum = \Phi_{r_1 r_2} = \sum_{r_1^2 \leqslant u^2+v^2 \prec r_2^2} |F(u,v)|^2$$

$$Angular\ Sum = \Phi_{\theta_1,\theta_2} = \sum_{\theta_1 \leqslant \tan^{-1}(v/u) \leqslant \theta_2} |F(u,v)|^2$$

A.3.3. Gabor Filter based Features

$$Mean = \frac{1}{m}\sum_{i} iP_{ij}$$

$$\text{Variance} = \sum_{i,j} P_{i,j}(i - \mu_i)^2$$

Appendix-B

Plagiarism Report

ORIGINALITY REPORT

9 %	4 %	7 %	0 %
Similarity Index	Internet Sources	Publications	Student Papers

PRIMARY SOURCES

1	Virmani, Jitendra, Vinod Kumar, Naveen Kalra, and Niranjan Khandelwal. "Prediction of liver cirrhosis based on multiresolution texture descriptors from B-mode ultrasound", International Journal of Convergence Computing, 2013. Publication	1 %
2	Madasamy Raja, G. and Sadasivam, V. "Optimized local ternary patterns: a new texture model with set of optimal patterns for texture analysis", Journal of Computer Science, 2013. Publication	< 1%
3	www.ecn.nl Internet Source	< 1 %
4	Subashini, T.S. " Automated assessment of breast tissue density in digital mammograms", Computer Vision and Image Understanding, 201001 Publication	< 1 %
5	Singh, Harpreet and Sumeet Dua. "Supervised Classification of Digital Mammograms", Data Mining in Biomedical Imaging Signaling and Systems, 2011. Publication	< 1 %
6	Peters, Stefanie. "Automatischer Entwurf und Autokonfiguration von Bildverarbeitungssystemen für die industrielle Oberflächeninspektion", KLUEDO, 2011. Publication	< 1 %
7	Bansal, Maggi, Vipul Sharma, and Sukhwinder Singh. "Comparison of texture models for efficient ultrasound image retrieval", Medical Imaging 2013 Computer-Aided Diagnosis, 2013. Publication	< 1 %
8	etd.rau.ac.za Internet Source	< 1 %
9	Virmani, Jitendra, Vinod Kumar, Naveen Kalra, and Niranjan Khandelwal. "SVM-based characterisation of liver cirrhosis by singular value decomposition of GLCM matrix", International Journal of Artificial Intelligence and Soft Computing, 2013. Publication	< 1 %
10	eia.udg.es Internet Source	< 1 %
11	www.scribd.com Internet Source	< 1 %
12	www.eng.iastate.edu Internet Source	< 1 %
13	jcc2011.utalca.cl Internet Source	< 1 %

14	ehealthlab.cs.ucy.ac.cy Internet Source	< 1 %
15	www.vcl.fer.hr Internet Source	< 1 %
16	www.eclac.org Internet Source	< 1 %
17	ssa.nic.in Internet Source	< 1 %
18	www.ijera.com Internet Source	< 1 %
19	Aylward, Stephen, Lubomir M. Hadjiiski, Yan Nei Law, Monica Keiko Lieng, Jingmei Li, and David Aik-Aun Khoo. "Automated breast tissue density assessment using high order regional texture descriptors in mammography", Medical Imaging 2014 Computer-Aided Diagnosis, 2014. Publication	< 1 %
20	archive.org Internet Source	< 1 %
21	Joana Lopes da Fonseca. "Pre-CADs in Breast Cancer", Repositório Aberto da Universidade do Porto, 2013. Publication	< 1 %
22	www.mathworks.com Internet Source	< 1 %
23	Rita Teixeira. "Automatic Analysis of Mammography Images: Classification of Breast Density", Repositório Aberto da Universidade do Porto, 2013. Publication	< 1 %
24	siimcenter.org Internet Source	< 1 %
25	biosim.ece.ntua.gr Internet Source	< 1%
26	Llobet, Rafael, Marina Pollán, Joaquín Antón, Josefa Miranda-García, María Casals, Inmaculada Martínez, Francisco Ruiz-Perales, Beatriz Pérez-Gómez, Dolores Salas-Trejo, and Juan-Carlos Pérez-Cortés."Semi-automated and fully automated mammographic density measurement and breast cancer risk prediction", Computer Methods and Programs in Biomedicine, 2014. Publication	< 1 %
27	ojs.academypublisher.com Internet Source	< 1 %
28	Quintana, C., M. Redondo, and G. Tirao. "Implementation of several mathematical algorithms to breast tissue density classification", Radiation Physics and Chemistry, 2013. Publication	< 1 %
29	Sérgio Koodi Kinoshita. "Content-based Retrieval of Mammograms Using Visual Features Related to Breast Density Patterns", Journal of Digital Imaging, 05/15/2007 Publication	< 1 %
30	Li, Jun-Bao, Yun-Heng Wang, and Lin-Lin Tang. "Mammogram-based discriminant fusion analysis for breast cancer diagnosis", Clinical Imaging, 2012. Publication	< 1 %